Deep pacific circulation: New insights on pathways through the Solomon Sea

C. Germineaud, S. Cravatte, J. Sprintall, M. S. Alberty, M. Grenier, A. Ganachaud

Deep Sea Research Part I: Oceanographic Research Papers
May 2021, Volume 171, Pages 103510 (15p.)
https://doi.org/10.1016/j.dsr.2021.103510
https://archimer.ifremer.fr/doc/00685/79704/

Deep pacific circulation: New insights on pathways through the Solomon Sea

Germineaud C. [1, 2, *], Cravatte S. [3], Sprintall J. [4], Alberty M.S. [5], Grenier M. [3], Ganachaud A. [3]

[1] Cooperative Institute for Marine and Atmospheric Studies, University of Miami, Miami, FL, USA
[2] NOAA/Atlantic Oceanographic and Meteorological Laboratory, Physical Oceanography Division, Miami, FL, USA
[3] Laboratoire d'Etudes en Géophysique et Océanographie Spatiales, Université de Toulouse, CNES, CNRS, IRD, UPS, Toulouse, France
[4] Scripps Institution of Oceanography, University of California, San Diego, CA, USA
[5] Geophysical Fluid Dynamics Laboratory, Princeton University, Princeton, NJ, USA

* Corresponding author : C. Germineaud, email address, cyril.germineaud@gmail.com

Abstract :

In the South Pacific Ocean, upper and lower Circumpolar Deep Water (UCDW and LCDW, respectively) occupy the deep layers; however, the presence and fate of both these water masses in the western equatorial Pacific have been mostly based on sparse measurements in both space and time. In this study, unprecedented deep measurements from three cruises conducted in the Solomon Sea region along with the World Ocean Atlas 2018 database are examined to better characterize the properties and pathways of deep water in the Southwest Pacific. At depths encompassing most of the UCDW, estimated transports derived from two inverse model solutions indicate interbasin exchanges between the Solomon Sea Basin and the Coral Sea Basin to the south and the East Caroline Basin to the north. The deep water transport variability found across the Solomon Sea is consistent with observed water mass modifications due, for the most part, to diapycnal mixing. At depths greater than about 2600 m, deep water inflow into the Solomon Sea Basin is limited to the south, emanating from the Coral Sea remote basins via complex trench topography. Spreading of LCDW in the Coral Sea and subsequently into the Solomon Sea is blocked by the Tonga-Kermadec Ridge to the east and bottom topography to the south, however, the densest part of UCDW entering both the Coral and Solomon Seas is likely influenced by LCDW properties, as oxygen is found to increase and silicate decrease with depth in the region. Waters trapped in closed deep basins, in the Bismarck Sea below 1750 m and the northern Solomon Sea below 3500 m show a remarkably constant pattern in oxygen with depth.

Highlights

► Solomon Sea deep waters are supplied from the Coral Sea and East Caroline Basins. ► Deep water transport variability is significant across the Solomon Sea. ► Deep water mass modifications are due to diapycnal exchanges in the Solomon Sea.

Keywords : Deep water masses, Southwest Pacific, Throughflow variability, Diapycnal mixing

1 Introduction

Over the past decade, several studies have highlighted the key contribution of the deep (2000-4000 m) and abyssal (depths > 4000 m) oceans in accumulating excess heat from the surface (e.g., Johnson et al., 2015; Purkey and Johnson, 2010), with large contributions from the Southern Ocean and the South Pacific Ocean (Desbruyères et al., 2016; Purkey et al., 2019; Meinen et al., 2020). However, to be able to properly assess and monitor this observed heat uptake from the oceans below 2000 m, it is important to have a better understanding of the water circulation and properties in the deep and abyssal layers. In the Pacific Ocean, the abyssal waters originate from the Southern Ocean, as a mixture between dense and cold water from the Antarctic Bottom Water (AABW) and the densest part of the overlaying Circumpolar Deep Water (CDW) at the northern edges of the Antarctic Circumpolar Current (ACC; Mantyla and Reid, 1983; Orsi et al., 1999; Johnson, 2008). Most of this mixture enters the Pacific Ocean via the Southwest Pacific Basin, the only major basin that remains open to the Northern Hemisphere below 3500 m (see Fig. 1; Tsimplis et al., 1998).

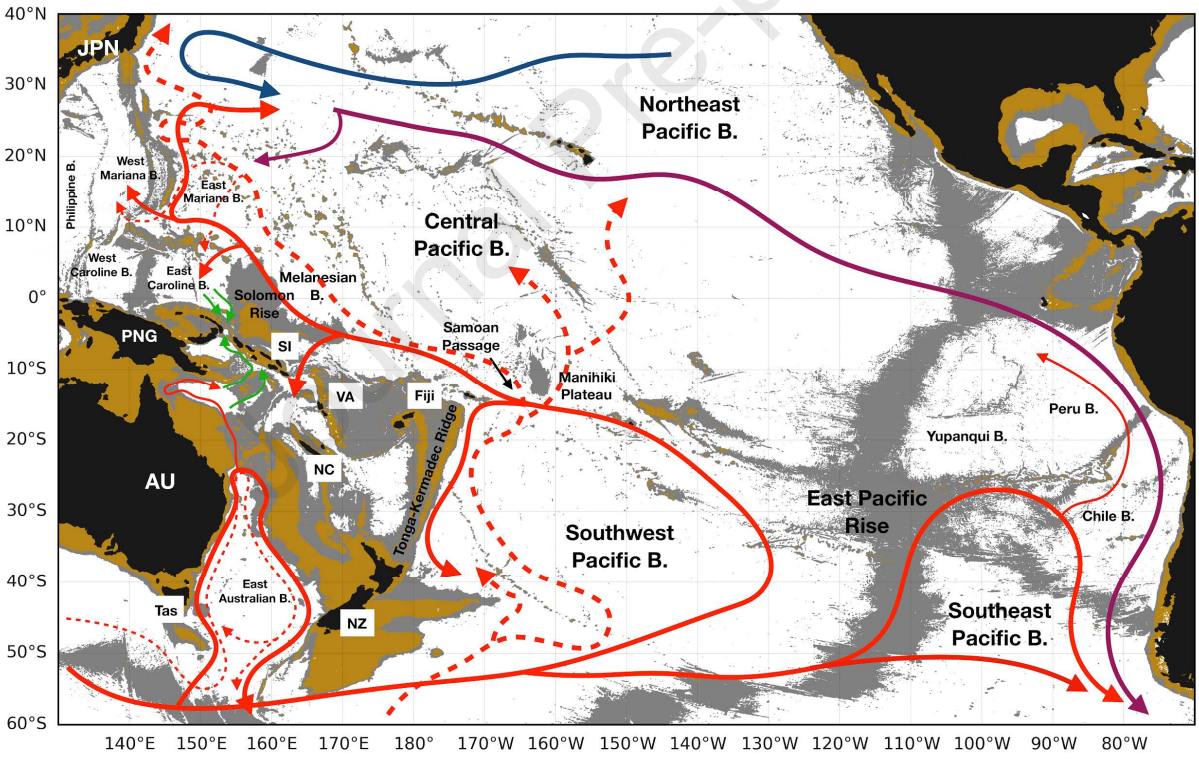

Fig. 1: Map of the Pacific Ocean south of 40°N. Brown shading shows bathymetry above 2000 m; gray shading indicates areas at depths of 2000 to 3500 m from the gridded 30 arc-second General Bathymetric Chart of the Oceans (GEBCO) 2020. Solid red lines with arrows indicate schematic pathways of the Upper Circumpolar Deep Water (UCDW); solid blue line shows the flow of North Pacific Deep Water (NPDW) and solid purple lines indicate modified NPDW flow. These pathways are based on the study of Siedler et al. (2004) and Figure 2b of Kawabe and Fujio (2010). Paths of the Lower Circumpolar Deep Water (LCDW) are in dashed red lines based on Figure 2c of Kawabe and Fujio (2010), Figure 15 of Siedler et al. (2004) and Figure 16f of Sokolov and Rintoul (2000) in the East Australian Basin, in which the thin solid red line represents the Antarctic Circumpolar Current bottom water

(ACCbw). Schematic pathways of UCDW above sill depths into the Solomon Sea Basin (green lines with arrows) based on this study are also indicated. Country/Island names are indicated as follows: Australia (AU); Japan (JPN); New Caledonia (NC); New Zealand (NZ); Papua-New Guinea (PNG); Solomon Islands (SI); Tasmania (Tas) and Vanuatu (VA). Note that B. = Basin.

On the western boundary of the Southwest Pacific Basin, the Tonga-Kermadec Ridge prevents abyssal water inflow into the intricate and remote deep basins east of Australia, and subsequently into the Solomon Sea Basin, which is connected at great depths to the New Hebrides Basin via the South Solomon Trench (see Fig. 2 for locations). South of 12°S, the New Hebrides Basin is connected to the South Fiji Basin via the South New Hebrides Trench. At depths greater than 3000-3250 m, these basins are also isolated from the Central Pacific Basin, as possible inflow is blocked by shallow topography east of the Solomon Islands. North of 8°S, the Solomon Sea is strongly constrained by three narrow passages. The westernmost passage named Vitiaz Strait (147.6°E, 6°S) is closed to the north below a sill depth of 1070 m. To the east, St George's Channel (153.4°E, 4°S) has a sill depth of about 1400 m. The Solomon Strait (153.4°E, 4°S) is much deeper, but topography prevents flow paths deeper than 2600 m. The Solomon Sea was assumed to be isolated from the deeper thermohaline circulation pathways, and the ventilation of deep waters in this area, which at some locations reach depths greater than 9000 m, remains undocumented.

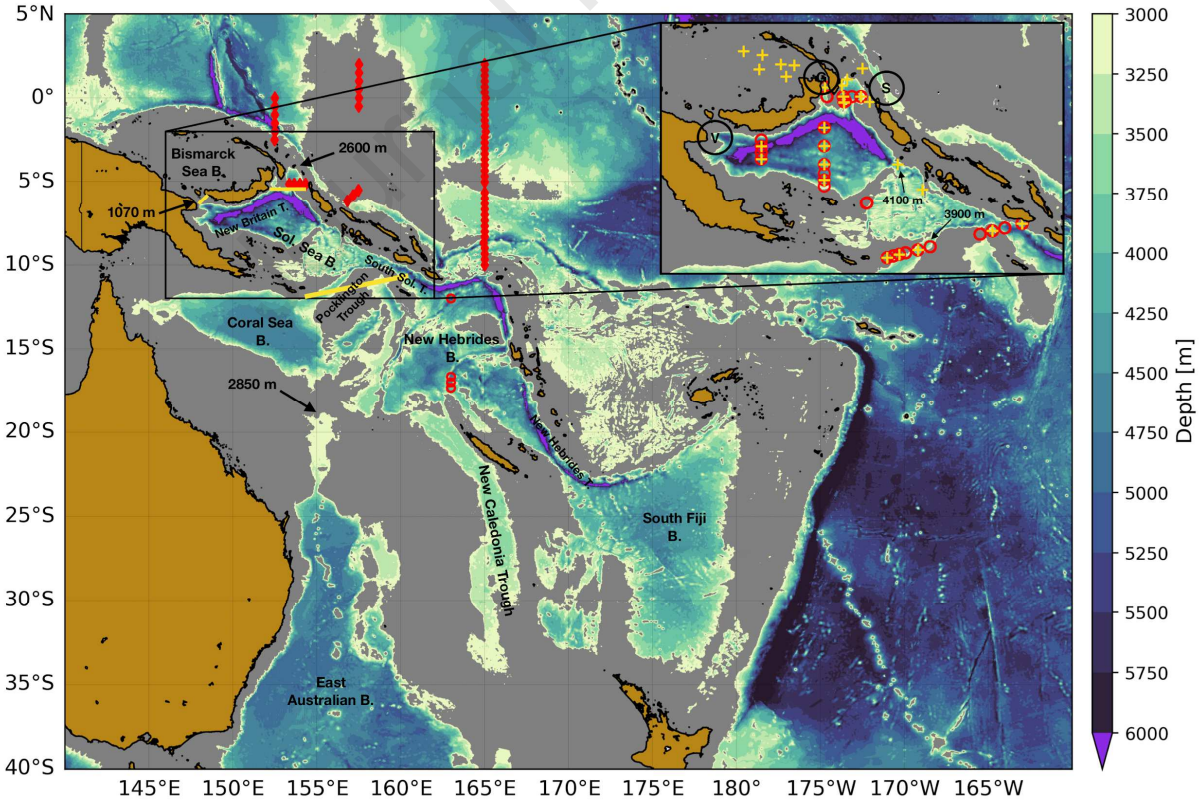

Fig. 2: Bathymetry below 3000 m of the western Pacific Ocean (140°E-160°W, 40°S-10°N) from the gridded 30 arc-second General Bathymetric Chart of the Oceans (GEBCO) 2020; the inset provides a

closer view of the Solomon Sea. Grey shading indicates locations where bathymetry (or bottom depth) is shallower than 3000 m, and critical sill depths (black arrows) are indicated. Hydrographic stations with measurements deeper than 2000 m depth are shown for the Pandora cruise (July 2012; red circles), MoorSPICE cruise (March 2014; yellow crosses) and Cassiopée cruise (July-August 2015; red diamonds). The transects defining the boundaries of the inverse model are indicated as yellow lines; the circled V, S and G (see inset) represent Vitiaz Strait, Solomon Strait, and St George's Channel, respectively. Sol. = Solomon; B. = Basin and T. = Trench.

Hydrographic data in the subtropical Pacific have been previously limited to four main sections (http://whp-atlas.ucsd.edu/pacific/sections.htm) collected in the 1990s as part of the World Ocean Circulation Experiment (WOCE): the P06 (153.3°E-71.5°W, 30°S-32°S), P11S (155°E, 11.4°S-43.2°S), P14C (175.2°E-177.6°E, 18.3°S-35.4°S) and P21 (153.4°E-75.1°W, 15.3°S-24.6°S). More recently, these sections were reoccupied under the international Global Ocean Ship-based Hydrographic Investigations Program (GO-SHIP), but a large part of the deep and abyssal waters in the western equatorial Pacific (145°E-165°W, 15°S-15°N) remains poorly sampled, or even completely unexplored. Indeed, a comprehensive set of *in situ* hydrographic measurements in the Solomon Sea region was, until recent years, mostly based on a few full-depth observations collected during the Western Equatorial Pacific Ocean Circulation Studies (WEPOCS) expeditions in the mid-1980s (e.g., Lindstrom et al., 1987).

As part of the Southwest Pacific Ocean Circulation and Climate Experiment (SPICE), two cruises extensively explored the Solomon Sea region in July 2012 and March 2014 (Ganachaud et al., 2017). Full-depth and high-resolution hydrographic transects were performed in the Solomon Sea and the surroundings during both cruises (see Fig. 2). A striking feature found during both cruises was the high oxygen signature in several occupied stations at depths greater than 3000 m in the Solomon Sea suggesting ventilation and the presence of the densest portion of the CDW. This new finding raises two main questions: (1) considering the topographic blockages, where does this deep water inflow come from? and (2) what are the water properties and the corresponding volume transport of this deep flow at the western boundary of the Southwest Pacific Basin?

Our study aims to investigate these two questions and give insights as to the broader implications of the deep and abyssal South Pacific Oceans. In the following, Section 2 will provide a background on our current understanding of the main deep water mass properties and their associated flow paths. In Section 3, we present the different datasets and methods of analysis. Section 4 describes the deep water mass properties in the western equatorial Pacific and provides transport estimates from inverse model solutions for each SPICE cruise. In Section 5, a comprehensive view of the deep water mass property distributions across the intricate Southwest Pacific region is discussed, before ending with some concluding remarks in Section 6.

2 Background: Deep Pacific Ocean circulation

At about 50°S from 150°E to 90°W, the Southern Ocean deep and bottom waters separate from the ACC and enter the South Pacific Ocean via the East Australian Basin, the Southwest Pacific Basin and the Southeast Pacific Basin (Fig. 1). In the Southern Ocean, Orsi et al. (2002) selected distinct neutral density surfaces (γ^n) to divide the deep ocean: 28.27 γ^n (~ 3000 m) to separate AABW from the lower part of the CDW (LCDW), 27.98 γ^n (~ 2000 m) marking the limit with the upper part of the CDW (UCDW), and 27.7 γ^n (~ 1000 m) defining the top of the UCDW. Note that in the ACC region, the densest layer of the LCDW ($28.18 < \gamma^n < 28.27$) is referred to as the ACC bottom water (ACCbw; Orsi et al., 1999). The ACCbw and the two portions of the CDW are exported into the South Pacific basins, however, the AABW is confined by the ridge systems south of 50°S (Orsi et al., 1999). In the following, our current knowledge of the pathways and relevant water mass properties associated with the ACCbw and the two portions of the CDW across the Pacific Ocean are presented. The distinct property values identified in past studies to trace these deep water masses vary with latitude across the western Pacific Ocean; they are summarized for the region 145°E-165°W, 25°S-15°N in Table 1.

Water mass	**Depth (m)**	**Θ (°C)**	**S (PSS-78)**	**O_2 (µmol.kg^{-1})**	**SiO_4 (µmol.kg^{-1})**
UCDW	2000-3500	1.2-2.2	34.64-34.7	130-150	100-140
$NPDW_m$	2000-3500	1.2-2	34.58-34.68	110-130	140-155
LCDW	3500+ m	< 1.2	34.685-34.73	> 155	110-142

Table 1: Characteristics of known deep water types in the Pacific Ocean north of 25°S to 15°N. Boundaries of UCDW properties are derived from Kawabe et al. (2009) and Sokolov and Rintoul (2000); The $NPDW_m$ and LCDW properties are based on corresponding property values identified by Siedler et al. (2004) and Wijffels et al. (1998).

2.1 Antarctic Circumpolar Current bottom water and Lower Circumpolar Deep Water

In the East Australian Basin, both the ACCbw and LCDW are blocked by topography north of 20°S (Sokolov and Rintoul, 2000), and so turn southward and ultimately recirculate northwestward along the coast of Tasmania (Tsimplis et al., 1998) or feedback to the ACC system (red dashed lines in Fig. 1). East of the East Pacific Rise, the ACCbw is confined to the Southeast Pacific Basin, while the lightest LCDW is able to proceed northeastward into the Chile Basin, and then into the Peru Basin over sills shallower than 4000 m (Tsimplis et al., 1998). Most of the ACCbw and LCDW are transported in the Southwest Pacific Basin as a Deep Western Boundary Current (DWBC) along the Tonga-Kermadec Ridge (Whitworth III et al., 1999).

Around 10°S, LCDW enters the Central Pacific Basin through the Samoan Passage and along the eastern side of the Manihiki Plateau (Roemmich et al., 1996; Rudnick, 1997; Voet et al., 2014,

2016), while ACCbw is blocked south of the Samoan Passage (Orsi et al., 1999) and returns southward (Reid, 1997).

At depths greater than 3500 m, LCDW is found below potential temperatures of $\theta = 1.2°C$ (Siedler et al., 2004; Kawabe and Fujio, 2010), and is characterized by a salinity (S) maximum and a silicate (SiO_4) minimum (Orsi et al., 1999; Warren, 1973). Along the zonal WOCE P06 section in the Southwest Pacific, Whitworth III et al. (1999) found high dissolved oxygen (O_2) concentrations (180-214 $\mu mol.kg^{-1}$) associated with LCDW, while north, in the East Mariana Basin, the O_2 concentration below 3500 m only reaches values between 155 to 180 $\mu mol.kg^{-1}$ (Siedler et al., 2004; Wijffels et al., 1998). As LCDW proceeds northward within the Central Pacific Basin, it splits into two branches, which eventually reach the Northeast Pacific Basin via complicated and narrow passages (e.g., Siedler et al., 2004; Kawabe et al., 2006). On its northern route, the LCDW accumulates silicate from bottom sediments (Alford et al., 2013; Talley and Joyce, 1992; Toole et al., 1994; Roemmich et al., 1996), associated with a decrease in O_2 before being upwelled in the upper deep layers and ultimately transformed into North Pacific Deep Water (NPDW) via diapycnal mixing north of 40°N (e.g., Johnson et al., 2006).

These previous studies provide good overall pictures of the ACCbw and LCDW pathways and associated water properties in the Pacific Ocean; however, it is apparent that more detailed and accurate views of the circulation at near-bottom levels warrant further investigation. In this study, our results will confirm that LCDW does not spread to the Southwest Pacific basins, but it can imprint the overlying UCDW with its high oxygen signature.

2.2 Upper Circumpolar Deep Water and North Pacific Deep Water

According to previous studies, UCDW is characterized by an O_2 minimum (Callahan, 1972; Talley et al., 2007) and nutrient maxima (Warren, 1973; Whitworth III et al., 1999). At about 20°S in the East Australian Basin, UCDW enters the Coral Sea with a transport of 3 Sv (Sokolov and Rintoul, 2000) based on the observations of the WOCE P11 section. Sokolov and Rintoul (2000) suggested that UCDW found in the eastern part of the Coral Sea is primarily supplied by waters coming from the Central Pacific Basin, and that UCDW entering from the east may flow into the South Solomon Trench, before continuing northward across the Solomon Sea (Sokolov and Rintoul, 2000; see their Figure 16f).

Nevertheless, the path of this deep inflow is rather uncertain as it is based on relatively scarce measurements. The θ-S curves described by Sokolov and Rintoul (2000; their Figure 12) within the Solomon Sea, at Vitiaz Strait, St George's Channel, Solomon Strait and in the New Britain Trench were similar to those shown for the South Solomon Trench. This indicated homogeneous distributions of water mass properties throughout the Solomon Sea, which were cooler and fresher than those entering the Coral Sea further to the South from the East Australian Basin. Additionally, clear differences in both θ and S between the East Caroline Basin and the northern

part of the Solomon Sea suggested a limited deep inflow of northern origin through the Solomon Strait. As shown below, the results of the two SPICE cruises and Cassiopée rather suggest that exchanges of UCDW between the Solomon Sea Basin and the East Caroline Basin can occur, and that the primary source of UCDW in the Solomon Sea is the Coral Sea Basin, as initially suggested by Wyrtki (1961).

At about 50°S east of 120°W, UCDW can enter the Southeast Pacific Basin before continuing northeastward into the Chile Basin (Fig. 1). Although the UCDW waters might proceed further north into the Peru and Yupanqui Basins, since there is no blocking bathymetry, previous studies (e.g., Reid, 1986, 1997; Tsimplis et al., 1998) indicated that most of the UCDW turns southward near the coasts of South America before returning to the ACC. From 40°S to 10°S, west of 120°W, an anticyclonic flow, which corresponds to the lower limb of the subtropical gyre, occupies the Southwest Pacific Basin at depths of about 2000 to 3500 m (Reid, 1997; Kawabe and Fujio, 2010). As the UCDW flows into the Southwest Pacific Basin (red solid lines in Fig. 1), waters are passing around the subtropical gyre before crossing the Samoan Passage (e.g., Roemmich et al., 1996; Rudnick, 1997; Taft et al., 1991), though part of the UCDW flows southward along the Tonga-Kermadec Ridge and recirculates in the subtropical gyre (Reid, 1997). Around 10°S, UCDW bifurcates northwestward and flows around the Solomon Rise (Fig. 1), before reaching the East Caroline Basin and the East Mariana Basin found north of the Solomon Sea (Kawabe et al., 2006, 2009). UCDW proceeds northward in the North Pacific and enters the Philippine Sea. Then, UCDW spans eastward towards the Hawaiian Ridge, where it meets NPDW that flows eastward from the north near 30°N (Kawabe et al., 2009; Kawabe and Fujio, 2010).

As mentioned in the previous section, the NPDW is formed through mixing as LCDW upwells in the North Pacific, with the imprint of a strong SiO_4 content (> 170 $\mu mol.kg^{-1}$) from the seabed (Talley and Joyce, 1992; Talley et al., 2007). Most of the NPDW can be traced through its SiO_4-rich signature as it flows westward into the Northwest Pacific Basin, and then southward at about 170°W (Johnson et al., 2006; Kawabe and Fujio, 2010). UCDW and NPDW signatures converge around 25°N-170°E to ultimately form a modified NPDW (hereinafter $NPDW_m$) that proceeds southeastward (eastward purple line in Fig. 1) in the eastern Pacific before encountering the South American coastline, and flows southward into the ACC in the Drake Passage (Kawabe et al., 2009; Talley et al., 2007). Previous studies (Johnson and Toole, 1993; Siedler et al., 2004) have also found high-SiO_4 concentrations in the Northwest Pacific around 15°N, suggesting possible transport of $NPDW_m$ from the east to the southeastern boundary of the East Mariana Basin, and potentially also entering the East Caroline Basin (westward purple line in Fig. 1).

3 Data and Inverse Model

3.1 Ocean historical, bathymetry and cruise data

This study takes advantage of both historical measurements of θ (calculated using the *in situ* temperature and absolute salinity fields, and a reference pressure at 0 dbar), S, O_2 and nutrients from the World Ocean Atlas 2018 (WOA18; https://www.nodc.noaa.gov/OC5/woa18/pubwoa18.html) collected from January 1, 1950 to December 31, 2018. Only profiles below 2000 m depth from the Ocean Station Data (OSD) and high-resolution Conductivity-Temperature-Depth (CTD) datasets in the western Pacific Ocean (120°E-160°W, 50°S-10°N) were considered here. Of these profiles, only those with quality flags indicating good data were considered.

To determine potential deep pathways in the Southwest Pacific region, areas associated with critical sill depths and relevant topographic blockages are identified using the General Bathymetric Chart of the Oceans (GEBCO) gridded dataset (GEBCO Compilation Group, 2020), as well as *in situ* echo-sounding surveys available from the two SPICE cruises.

Under the SPICE program, the first cruise (known as Pandora on the *R/V L'Atalante*) was conducted from 27 June to 6 August 2012 along a meridional transect north of Nouméa (163°E, from 18°S to 9°S) and across the Solomon Sea (Fig. S1), while the second cruise (known as MoorSPICE on the *R/V Thomas G. Thompson*) explored both the Solomon Sea and the Bismarck Sea from 28 February to 31 March 2014 (Fig. S1). Overall, 83 and 57 stations were surveyed during Pandora and MoorSPICE, respectively. A thorough description of the collected data and associated processing is available in Ganachaud et al. (2017); we only present here relevant information for this study. It is also worth mentioning that nine subsurface moorings were deployed from July 2012 until March 2014 at Vitiaz Strait, St George's Channel and Solomon Strait to determine the distinct cross-passage flow variability (Alberty et al., 2019). However, the moored hydrographic and current measurements recorded at the deepest channel of Solomon Strait are limited to a maximum depth of 1700 m and so are not employed here. A third cruise (known as Cassiopée on the *R/V L'Atalante*) was conducted from 19 July to 23 August 2015 (Delpech et al., 2020); during which 74 hydrographic stations were occupied north and east of the islands bounding the Solomon Sea, with three meridional transects performed at approximately 153.5°E, 157.7°E and at 165°E (Fig. S1).

During these three cruises, T, S and O_2 measurements were carried out using CTD and O_2 sensors, and a pair of Lowered-Acoustic Doppler Current Profilers (L-ADCPs) to measure currents. The pair of L-ADCPs was processed following Visbeck (2002). Absolute velocities were estimated using a least squares framework, including constraints on bottom velocity estimates from bottom-track pulses, navigational data and upper ocean velocities from the along-track shipboard ADCP data.

Discrete water samples were also obtained during the cruises with Niskin bottles to calibrate the CTD-O_2 sensors (S and O_2) and for nutrient (nitrate NO_3, phosphate PO_4 and SiO_4)

determination. A specific calibration was carried out for the O_2 sensor data by comparison with a Winkler titration determination of the water samples (Langdon, 2010; Uchida et al., 2010; Saout-Grit et al., 2015). During Pandora, 39 of the 164 casts were taken to depths greater than 2000 m (red circles in Fig. 2), including repeat time series casts at 10 stations. During MoorSPICE, 30 of the 82 casts were carried out deeper than 2000 m (yellow crosses in Fig. 2) with repeat casts at 16 stations, while during Cassiopée, 56 of the 98 casts were deeper than 2000 m (red diamonds in Fig. 2), and 26 stations were occupied multiple times.

The collected measurements during the three cruises were quality controlled following the GO-SHIP guidelines (Hood et al., 2010). We use in this study the cruise measurements identified as "good data" for the CTD-O_2 profiles, and as "probably good data" ("good data" flag is not available) for the bottle water samples. It should also be noted that we only use here the SiO_4 samples collected during Pandora, because some measurement issues were found with the SiO_4 samples from the MoorSPICE and Cassiopée cruises at depths greater than 2000 m. Data from all three cruises are used to describe the water property characteristics of the deep waters but only the Pandora and MoorSPICE cruises are used in the inverse model. This is because, unlike the two SPICE cruises, the hydrographic transects performed during the Cassiopée cruise do not enclose the Solomon Sea across the entrances and exits.

3.2 Inverse Model

3.2.1 Inversion Principle

Linear inverse methods applied to hydrographic measurements (e.g., Ganachaud and Wunsch, 2000; Lumpkin and Speer, 2007; Germineaud et al., 2016) have been extensively used to estimate ocean circulation and associated transports within a finite ocean volume divided in different layers from the surface down to the bottom, and usually chosen to encompass major water masses. The classical procedure uses pairs of *in situ* temperature and salinity profiles along hydrographic transects to calculate an initial guess of geostrophic flow relative to a given reference level along with *a priori* velocity uncertainties, which can be, in practice, estimated from deep current meters or L-ADCP profiles. One can then use an inverse method to estimate an adjusted velocity field and corresponding transports with uncertainties to depict a more synoptic representation of the ocean circulation than the one inferred from the initial observed velocities. For this purpose, adjustments to the initial guess (*a priori* velocities) are typically made such that the revised circulation scheme satisfies basic conservation requirements of the total mass transport and water property fluxes (e.g., salt, heat and/or nutrients).

3.2.2 Our Inverse Model

Within the Solomon Sea, an inverse model based on Gauss-Markov estimation (Wunsch, 1996), is used to estimate synoptic transports of the deep flow during Pandora and MoorSPICE across three hydrographic transects enclosing the Solomon Sea (yellow lines in Fig. 2). Mass and

property constraints are applied over 25 and 24 (during Pandora and MoorSPICE, respectively) isopycnal layers defined by potential density anomaly surfaces to derive adjusted velocities and transports with error estimates. The *a priori* velocities and the different model's constraints are presented in the two following sections. As we focus on the deep circulation here, we will only present the nonadjusted (before inversion) and adjusted (after inversion) transports across the Solomon Sea for the deep layers, at depths greater than 1500 m. Note that even though Vitiaz Strait is closed below 1000 m depth, our inverse model conserves mass top-to-bottom within the Solomon Sea box. The *a priori* transport estimates across Vitiaz Strait in the upper 1000 m are thus also taken into account to derive the two inverse model solutions.

3.2.3 Initial guess for the inverse calculation

For both the Pandora and MoorSPICE cruises, shipboard ADCP (S-ADCP) profiles are used as *a priori* velocities rather than geostrophic velocities to take into account current pathways as close as possible to the coast over the upper 1000 m in the Solomon Sea. In addition, the outflow through Vitiaz Strait, St George's Channel and Solomon Strait is constrained by processes other than geostrophy. At the southern entrance (south of 10°S), at depths where the S-ADCP is not available (i.e., below 1000 m), we use geostrophic velocities calculated between CTD station pairs, and then interpolated on the S-ADCP grid using a Gaussian weighting function. A vertical smoothing was performed using a 10-m moving average filter to avoid large discontinuities at the transition between S-ADCP and geostrophy.

The S-ADCP currents were rotated to be perpendicular to the transect (following Germineaud et al., 2016), then combined with the geostrophic velocity field. For the geostrophic part, an initial zero reference level was set at 3000 dbar, or, for shallower stations, at the deepest common level of station pairs along the transect at the southern entrance. L-ADCP profiles taken on CTD stations that were occupied more than once permitted the determination of initial reference velocities and associated uncertainties. Most of the cruise velocity profiles suggested velocities weaker than 5 cm s^{-1} at depths ranging from 2000 to about 3000 m, and so initial reference velocities were chosen to be 0 ± 5 cm s^{-1}. The outflow through Vitiaz Strait is limited to the upper 1000 m so only S-ADCP profiles are used as *a priori* velocities. To avoid estimates of unrealistic geostrophic flow across the northern transect between St George's Channel and Solomon Strait, a merged velocity field is built, based on S-ADCP velocities in the surface layer and L-ADCP profiles taken on CTD stations beneath the depth limit of the S-ADCP. Both S-ADCP and L-ADCP velocity profiles were first compared at overlapping depths, and only negligible discrepancies (< 1 cm s^{-1}) were observed. L-ADCP velocities were then interpolated onto the S-ADCP grid using the same Gaussian weighting function as used for the southern transect. This merged ADCP velocity field is used as our initial guess for the transect between St George's Channel and Solomon Strait. A range of velocity adjustments was set to 0 ± 5 cm s^{-1} based again on the repeated L-ADCP profiles recorded on stations along the section. Note that a similar ADCP velocity field was also built for the southern transect; however, large uncertainties

in bottom track velocity estimates from the two paired L-ADCPs (especially during MoorSPICE) led to spurious strong velocities (> 15 cm s^{-1}) at the deepest measurements.

We estimate the upper deep layer transport with uncertainties across the transect at the southern entrance and at the northeastern exit (through both St George's Channel and Solomon Strait), in one primary isopycnal layer bounded by 27.65 and 27.76 σ_0 (Table 2). The isopycnal σ_0 = 27.65 (~ 2000 m) is above θ = 2.2°C, which marks the transition of the lighter deep layer mixed with intermediate waters. Below, σ_0 = 27.76 (~ 3250 m) approximately corresponds to the transition from low to increasing S and O_2. Both initial (before inversion) and adjusted (after inversion) transports are reported (see Table 2).

3.2.4 Constraints on the adjusted flow

The adjusted velocity field described above during both the MoorSPICE and Pandora cruises is estimated so that conservation requirements on mass, heat, salt are met over the whole water column. Vertical advective (w) and diffusive (κ_z) exchanges are allowed between isopycnal layers, which were chosen to have a relatively homogeneous thickness over the basin, as well as freshwater and Ekman fluxes (see Germineaud et al., 2016 for further detail). For the Pandora cruise, where silicate data is available, silicate content is conserved from the surface down to the deepest layers but not within individual layers, as it is expected to be nearly conservative within a top-to-bottom oceanic volume enclosed by hydrographic transects (Ganachaud and Wunsch, 2002).

For both the Pandora and MoorSPICE cruises, *a priori* uncertainties of mass are set following Germineaud et al., (2016), with larger uncertainties (± 2 Sv instead of ± 1 Sv) near the surface and in the deepest layer, allowing exchanges with abyssal waters (σ_0 > 27.76). Heat and salt are also not conserved in the surface and deepest layers, using anomaly equations and associated scaling factors (following Ganachaud, 2003). All constraints were met within uncertainties, and the estimated velocities adjusted to the deep reference level are below the initial velocity range ±5 cm s^{-1}. Even though both adjusted model solutions allow us to infer the circulation in the Solomon Sea at fairly high vertical resolution, it should be noted that their weaknesses include the assumption that the cruise data collectively provide a synoptic snapshot and possible bias is introduced by the data-based constraints used to adjust the initial guess through the inversion.

4 Deep water distributions in the Solomon Sea

4.1 Water mass properties

The deep waters properties are first investigated inside the Solomon and Bismarck Seas for waters between 2000 and 3500 m, corresponding to potential densities below σ_0 = 27.59 and above σ_0 = 27.78 (Fig. 3a). North of 25°S in the Southwest Pacific Basin to 15°N in the Central Pacific Basin, UCDW exhibits relatively low-O_2 (130-150 μmol.kg^{-1}) with θ and S values ranging

from 1.2° to 2.2°C and 34.64-34.7, respectively over the 2000-3500 m depth range (see Table 1). During the two SPICE cruises, corresponding UCDW properties are found in the Solomon Sea Basin, although there is a marked difference between the stations located in the northern part of the basin and those at the southern entrance. A distinction must also be made for waters with potential densities above σ_0 = 27.73 (~ 2600 m depth; bold dashed line in Fig. 3a), corresponding to the sill depth near Solomon Strait. To the north, within Solomon Strait (blue dots in Fig. 3), UCDW lighter than σ_0 = 27.73 is colder (blue dots in Fig. 3a), less oxygenated (Fig. 3b) and SiO_4-richer (Fig. 3c) than that at the southern entrance (red dots) and within the South Solomon Trench (magenta dots). The water properties at these depths in Solomon Strait are similar to those observed along the northern transects carried out at 153.5°E (green dots) and 157.7°E (black dots) during Cassiopée, indicating possible interbasin exchanges between the East Caroline Basin and the Solomon Sea Basin (at least in the northern part) below 2000 m and above the sill depth.

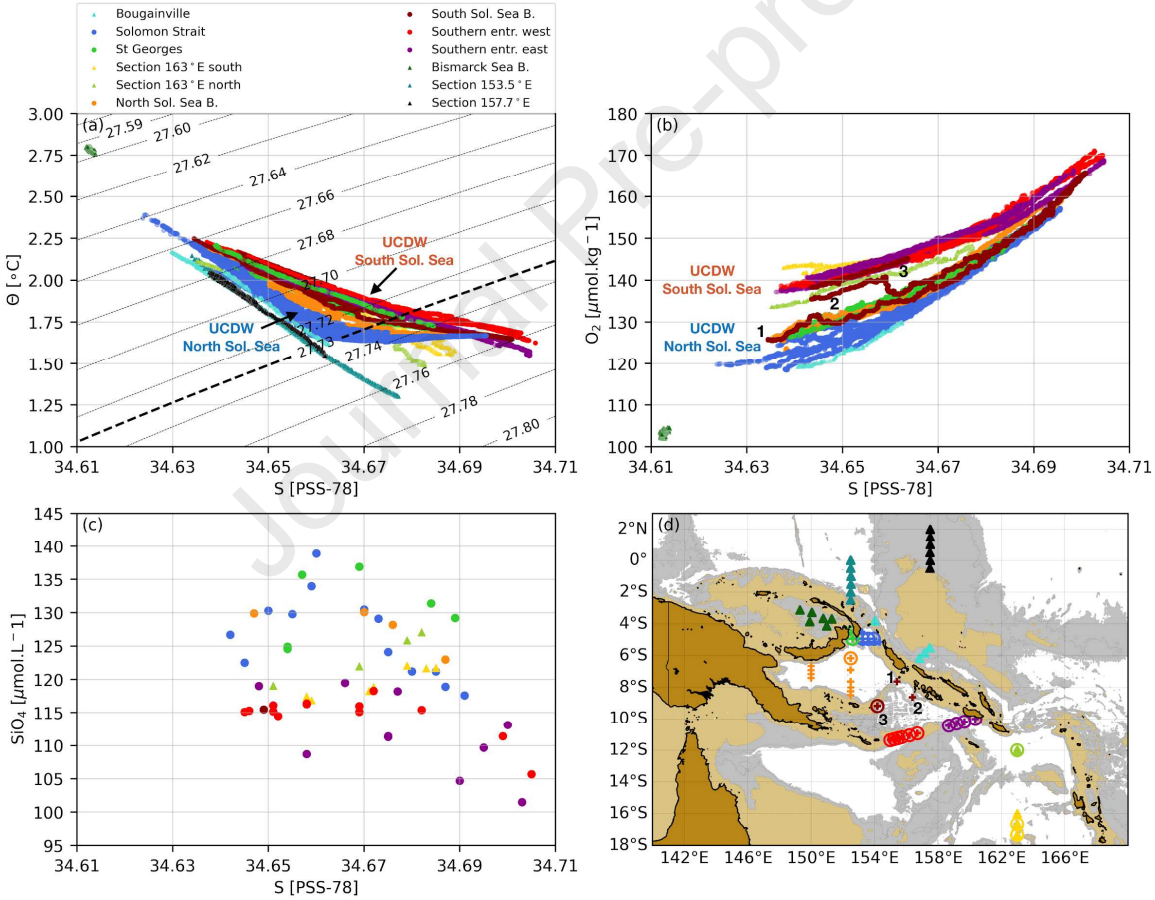

Fig. 3: Water mass property plots for measurements collected at depths between 2000 to 3500 m during the SPICE cruises and the Cassiopée cruise. (a) Potential temperature-salinity θ-S; bold dashed indicates the σ_0 level above which the East Caroline Basin and the Solomon Sea Basin remain connected, (b) dissolved oxygen-salinity O_2-S and (c) silicate-salinity SiO_4-S diagrams. Colors correspond to the locations as indicated in legend (top) in (a). The southern and northern origins of UCDW are also indicated; Sol. = Solomon; B. = Basin and entr. = entrance. Hydrographic stations are shown in (d), where

colored crosses indicate the CTD-O_2 casts, and colored circles indicate the bottle water samples. Note that the CTD-O_2 casts outside the Solomon Sea are shown as triangles instead of dots. The stations associated with the numbered O_2-S curves in (b) are indicated in (d). Light brown shading shows bathymetry above 2000 m, and gray shading indicates areas at depths of 2000 to 3500 m, as in Fig. 1.

Inside the northern part of the Solomon Sea, including near Vitiaz Strait and St George's Channel, waters appear to be a mixture between waters in Solomon Strait and waters entering from the south. This view is contrary to the tracer study of Sokolov and Rintoul (2000), although as mentioned before, only sparse observations of θ and S were available at the time of their study. During Pandora, the O_2 distributions along the transect at 163°E show similarly high-O_2 values to those found at the southern entrance of the Solomon Sea. This suggests that UCDW entering from the north through Solomon Strait is older than the UCDW entering the Solomon Sea from the south. Below $\sigma_0 = 27.73$, waters properties in the whole Solomon Sea Basin tend to have more consistent properties in θ and S as we go deeper in the water column, suggesting a unique origin. Yet, UCDW is slightly less oxygenated and SiO_4-richer in the northern part than at the southern entrance, suggesting older water, and a slower ventilation inside the basin. The evolution of the O_2-S curves within the southern part of the Solomon Sea (brown dots in Fig. 3b) further show that UCDW flowing there comes from the southern entrance, although some differences in property values are noted (see the numbered O_2-S curves and their respective locations in Figs. 3b, d). It also appears that an inflow of UCDW into the northern part of the basin is somewhat limited below $\sigma_0 = 27.72$ (~ 2400 m), i.e. the potential density at which a seesaw in O_2 near S = 34.66 is observed in the O_2-S curve numbered as 2 in Fig. 3b.

To investigate the different sources of UCDW into the Solomon Sea Basin, we use WOA18 property distributions (Fig. 4) at depths between 2000 to 3500 m for three possible origin regions: the Coral Sea Basin south of Papua New Guinea (orange dots in Fig. 4), east of the Solomon Sea in the Central Pacific Basin (170°E-180°, 5°S-10°S; blue dots in Fig. 4) and the East Caroline Basin (yellow dots in Fig. 4). While UCDW is warmer (Fig. 4a), more O_2-rich (Fig. 4b) and SiO_4-poor (Fig. 4c) in the Coral Sea Basin than that found in the Central Pacific, it has similar water property values to the UCDW found at the southern entrance of the Solomon Sea. This indicates that most of the UCDW entering the Solomon Sea Basin in the south comes primarily from the Coral Sea Basin rather than the Central Pacific Basin. This is consistent with the initial suggestion by Wyrtki (1961), but *a priori* not consistent with conclusions by Sokolov and Rintoul (2000). The latter authors concluded that waters entering the Solomon Sea (via the South Solomon Trench) mostly originated from the Central Pacific. Here, our results suggest that waters in the South Solomon Trench have properties similar to those in the Coral Sea Basin, and thus most likely originate from the Coral Sea Basin.

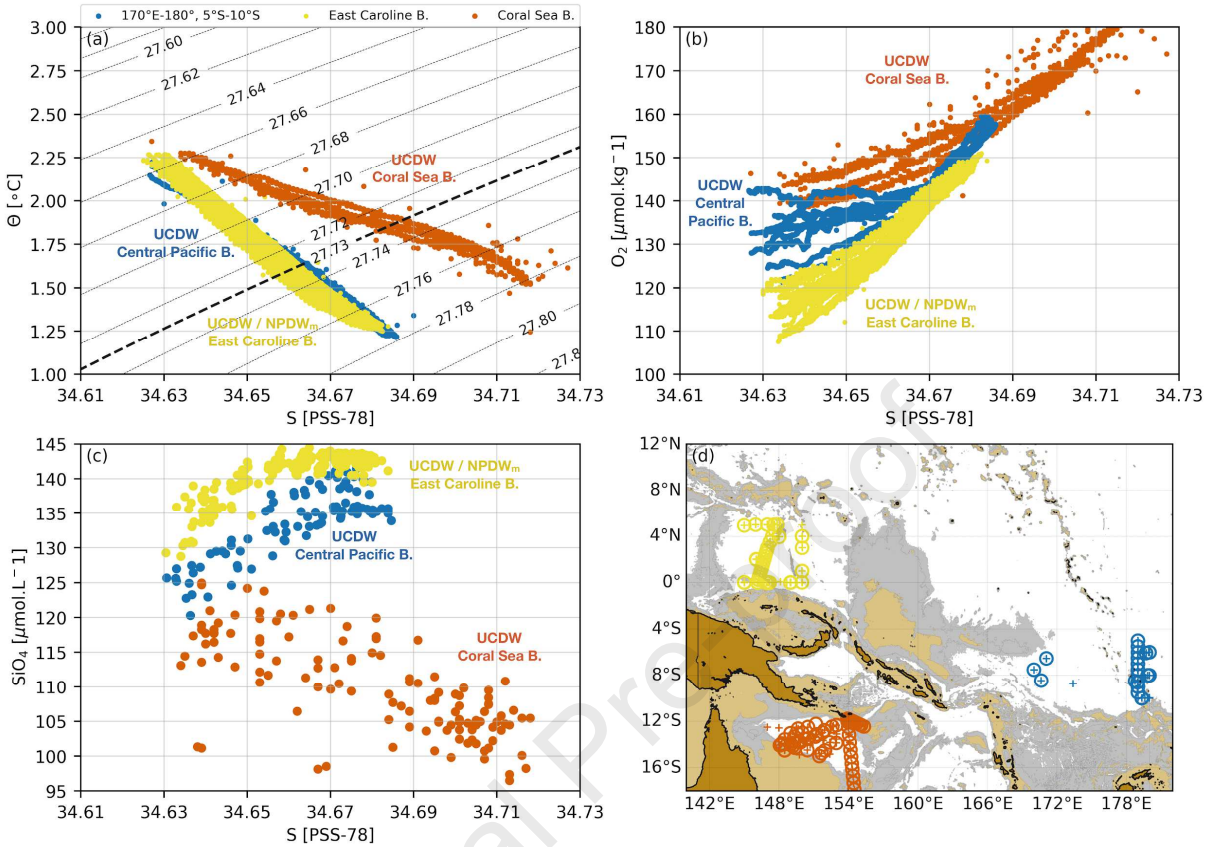

Fig. 4: Historical water mass property plots from WOA18 at depths between 2000 to 3500 m. (a) Potential temperature-salinity θ-S; bold dashed indicates the potential density anomaly σ_0 (kg m^{-3}; referenced to a sea pressure of zero dbar) level above which the East Caroline Basin and the Solomon Sea Basin remain connected, as in Fig. 3, (b) dissolved oxygen-salinity O_2-S and (c) silicate-salinity SiO_4-S diagrams. Colors correspond to the locations as indicated in legend (top) in (a). The deep water masses and origin are also indicated; B. = Basin. Hydrographic stations are shown in (d), where colored crosses indicate the CTD-O_2 casts and colored circles indicate the bottle water samples. Light brown shading shows bathymetry above 2000 m, and gray shading indicates areas at depths of 2000 to 3500 m, as in Fig. 1.

North, in the East Caroline Basin, we recognize a region of cold water (Fig. 4a), depleted in O_2 (Fig. 4b) and enriched in SiO_4 (Fig. 4c), indicating an NPDW$_m$ flow that most likely emanates from the neighboring East Mariana Basin located further north (where both basins remain connected above 4200-4300 m). Previous studies (e.g., Johnson et al., 1993; Siedler et al., 2004) have identified southward transports of NPDW$_m$ across the East Mariana Basin, suggesting that the East Caroline Basin is a region where UCDW and NPDW$_m$ mix; or at least, where incursions of NPDW$_m$ into the basin reinforce the low-O_2 and high-SiO_4 characteristic of the aged UCDW observed in that region. Finally, it is important to note that within the Bismarck Sea Basin (see Fig. 2 for location), which is no deeper than 2500 m, we do not observe (based on MoorSPICE data) any water mass properties corresponding to either UCDW or NPDW$_m$. Based on Figs. 3a

and 3b, the basin appears to be totally closed below 2000 m and exhibits completely homogeneous waters at all depths below 2000 m, which consist of warmer, fresher, and more O_2-poor water (cluster of dark green dots near S = 34.61 in Figs. 3a and 3b) than the deep waters encountered in the East Caroline and Solomon Sea Basins. The distributions of θ (Fig. S2a) and S (Fig. S2b) in the Bismarck Sea Basin at depths between 1000 to 1500 m are similar to those found in St George's Channel and Solomon Strait, while waters below 1750 m are vertically homogeneous throughout the Bismarck Sea Basin. It is thus clear that the Bismarck Sea Basin (which is in fact enclosed below 1750 m) is isolated from the deep circulation in the western equatorial Pacific at UCDW levels. Interestingly, the oxygen (Fig. S2c) remains constant with depth from 1750 to 2500 m, despite the lack of ventilation, while the nutrients (not shown) remain almost constant. While a detailed investigation of this constant pattern in both oxygen and nutrients is beyond the scope of this study, this suggests either that there is no oxygen consumption (remineralization) at depth, or that remineralization is compensated by downward diffusion of oxygen toward the deep ocean.

The deep water properties are further investigated for waters below 3500 m (Fig. 5), corresponding to potential densities below σ_0 = 27.78. In Fig. 5, the property values identifying the upper boundary of LCDW in the East Caroline Basin (i.e., θ < 1.2°C, S = 34.685, O_2 = 155 μmol.kg^{-1} and SiO_4 > 140 μmol.kg^{-1}; yellow dots) are found at depths below 4000 m, confirming similar conclusions by Seidler et al. (2004). From there, shallow topography prevents LCDW from proceeding westward into the West Caroline Basin and southward into the Solomon Sea Basin, as the East Caroline Basin is closed to the west and to the south below 3500 m. As no northern source exists for the bottom water in the Solomon Sea Basin, the densest water, that may originate as the lightest portion of LCDW, has to arrive from the south. In the Central Pacific Basin region (170°E-180°, 5°S-10°S; blue dots), water mass indicators marking the boundary between UCDW and LCDW are found at about 3750-4000 m, where θ < 1.2°C (Fig. 5a) is associated with a pattern of increasing O_2 (Fig. 5b) and decreasing SiO_4 (Fig. 5c). As expected, the LCDW at the western edge of the Central Pacific is more O_2-rich and SiO_4-poor than that found in the East Caroline Basin at those depths, reflecting the northward motion (and the aging) of LCDW there. Note that a LCDW inflow directly from the Central Pacific Basin into the Solomon Sea is expected to be blocked by topography, as the deepest narrow passages through the Solomon Islands do not exceed 3500 m depth.

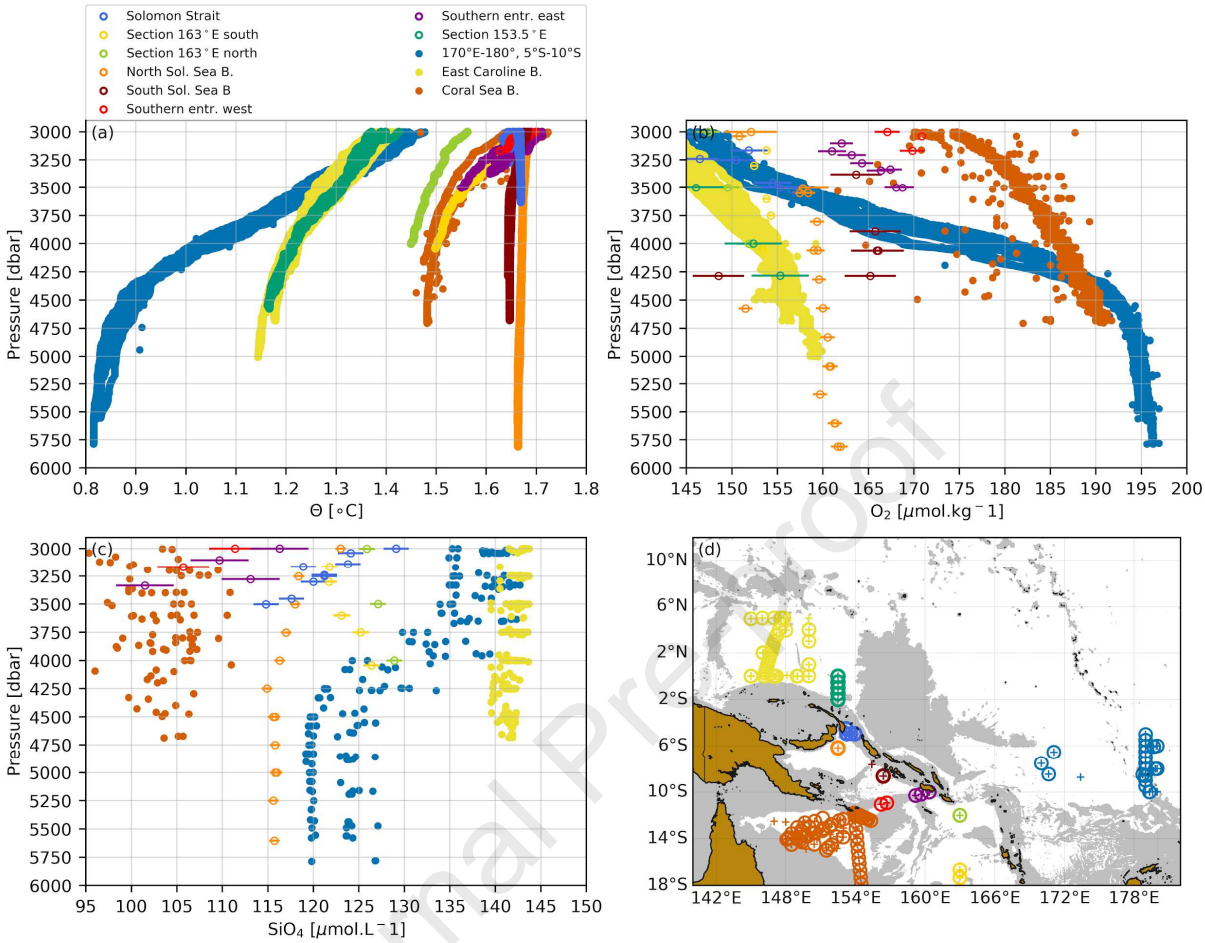

Fig. 5: (a-c) Vertical profiles with pressure (dbar) of potential temperature θ (°C; referenced to a sea pressure of zero dbar) in (a), dissolved oxygen O_2 (μmol.kg^{-1}) in (b) and silicate SiO_4 (μmol.kg^{-1}) in (c) from measurements collected at depths greater than 3000 m during the two SPICE cruises and Cassiopée (colored circles), and WOA18 (colored dots). Error bars associated with O_2 (b) and SiO_4 (c) from the SPICE cruises and Cassiopée were constructed from the standard error of the mean for each depth profile. Colors correspond to the locations as indicated in legend (top); Sol. = Solomon and B. = Basin and entr. = entrance. Hydrographic stations are shown in (d), where colored crosses indicate the CTD-O_2 casts, and colored circles indicate the bottle water samples. Gray shading indicates areas at depths greater than 3000 m.

Below 3500 m, we find θ values between 1.6° to 1.7°C at the deep stations occupied inside the southern and northern parts of the Solomon Sea Basin (see Fig. 5d for locations). These waters are warmer than all possible sources at the same depths. Waters in the Coral Sea Basin exhibit θ values from 1.45° to 1.55°C, consistent with observations from Wyrtki (1961) and Sokolov and Rintoul (2000), who found θ = 1.46°C for the deep waters in the Coral Sea Basin. Farther east, in the Central Pacific Basin, deep waters are much cooler (θ < 1.3°C). Several geothermal sources have been reported in the region (e.g., Halunen and von Herzen, 1973; Joshima and Honza, 1986), with a mean heat flow of about 85 mW.m^{-2} in the Solomon Sea Basin. However, note that

heating the water column over at least 1000 m above the seafloor by 0.15°C (assuming a constant heat flux of 85 $mW.m^{-2}$) would imply no water motion in the abyssal layer for about 530 years, which is unrealistic. As a geothermal source inside the Solomon Sea Basin able to heat waters at such great depths is not possible, this indicates that only the densest part of UCDW (i.e., above 3500 m depth and $\sigma_0 = 27.78$) can fill the deepest part of the basin. The O_2 (Fig. 5b), SiO_4 (Fig. 5c) and S (Fig. S3a) distributions also confirm these conclusions, although the values of O_2 in the Coral Sea Basin and the Central Pacific Basin are close to each other at depths between 3750 to 4750 m.

In the Solomon Sea Basin, for each cruise we observe nearly vertically uniform θ and S from 3500 m to the near-bottom depth, which may reflect strong diapycnal exchanges at those depths and/or long residence times for those water masses in the basin. Furthermore, only minor changes of θ (< 0.05°C; Fig. 5a) and O_2 (< 1.5 $\mu mol.kg^{-1}$; Fig. 5b) are found between the common stations from Pandora and MoorSPICE obtained during contrasting seasons, ruling out the possibility of significant seasonal variability. Corresponding changes in S can reach values of about 0.01 PSS-78 (Fig. S3a), with consistently higher S during MoorSPICE than found during Pandora. It is unclear though whether these observed salinity shifts reflect actual salinity variations or are calibration differences in conductivity sensors between both cruises, although comparisons of CTD S with bottle S were mostly within the manufacturer's accuracy specifications of the S sensor (<0.003 PSS-78). Either way, it appears that deep waters are vertically homogenized below 3500 m in the northern part of the Solomon Sea Basin, as confirmed by the vertical (and homogeneous) potential density profiles displayed in Fig. S4a.

A thorough analysis of the bottom topography in the Solomon Sea area (not shown) reveals that exchanges at depths reaching 3900 m are possible between the Coral Sea Basin and the southern Solomon Sea Basin via a deep narrow channel (known as the Pocklington Trough) located at the western end of the southern entrance (see Fig. 2 for location). Exchanges are also possible via the Solomon Sea Trough at the eastern end of the southern entrance of the Solomon Sea, with sill depths of about 4000 m. Between the southern and the northern parts of the Solomon Sea Basin, a narrow passage is possible at depths reaching 4100 m. Yet, it appears that these passages are too narrow to allow a significant water mass transport below 3500 m, and so the deep waters inside the Solomon Sea are not ventilated below 3500 m. Therefore, the apparent high-O_2 signal mentioned above is in fact a signature of high-O_2 UCDW waters originating from the Coral Sea Basin. The less O_2-rich (Fig. 5b) and the higher SiO_4 (Fig. 5c) characteristics in the northern part of the Solomon Sea Basin compared to the south is also an indicator of an aged inflow of dense UCDW coming from the Coral Sea Basin. In the Solomon Sea Basin, similar to the deep Bismarck Sea, it seems that there is little or no remineralization at depth, as both the oxygen and silicate remain constant locally below 3500 m.

4.2 Transports, mixing and variability

In the Solomon Sea box as defined by the sections across the inflow and outflow regions measured during the two SPICE cruises (Fig. 2), there is an adjusted transport needed across the southern section during the inversion. Most of the UCDW enters the box via two passages, a westward component between 156°E-157°E and one further east at 159°E-160°E between isopycnals ranging from 27.65 (~ 2000 m) to 27.76 (~ 3250 m) σ_0. For Pandora an adjustment of about 2.3 ± 1.7 Sv of UCDW across the southern transect is needed (Table 2). This equatorward adjusted transport of UCDW is halved during MoorSPICE (1.2 ± 0.7 Sv), possibly due to unaccounted net transport across the southern transect because CTD casts were shallower there during MoorSPICE compared to during Pandora. At the northern end of the Solomon Sea, the adjusted transport of UCDW across the transect joining St George's Channel and Solomon Strait amounts to 1.6 ± 1.7 Sv for Pandora and 1.4 ± 1.3 Sv for MoorSPICE (Table 2). The large uncertainty associated with these estimates suggests that transport could be either in or out of the basin, or rather close to zero at the UCDW levels. As noted before, the sill depth of St. George's Channel is 1400 m, and the sill depth out of Solomon Strait is 2600 m, implying that the transports below 2600 m are in fact necessarily zero.

Upper (σ_0, kg.m^{-3})	**Lower (σ_0, kg.m^{-3})**	**Southern entrance**	**St George's-Solomon**
27.65 (~ 2000 m)	27.76 (~ 3250 m)	**Before inversion** **Pandora:** 1.6 **MoorSPICE**: -0.1	**Before inversion** **Pandora:** 1.1 **MoorSPICE:** -1.8
		After inversion **Pandora:** 2.3 ± 1.7 **MoorSPICE**: 1.2 ± 0.7	**After inversion** **Pandora:** 1.6 ± 1.7 **MoorSPICE:** 1.4 ± 1.3

Table 2: Boundaries of the upper and lower ranges defining the deep waters and corresponding volume transports (Sv: 1 Sv ≡ 10^6 m^3 s^{-1}) during the Pandora and MoorSPICE cruises. Positive values indicate equatorward flow, negative values are southward and uncertainties are one standard deviation. After inversion transport estimates in and out the box are not exactly similar (2.3 vs. 1.6 Sv, 1.2 vs. 1.4 Sv), due to diapycnal fluxes to surrounding layers and residual noise.

Based on the assumption of synopticity of the measurements, the inverse-derived adjusted transports provide reliable estimates within errors, but it is useful to compare with the initial (nonadjusted) transports. At the southern entrance, the nonadjusted transport of UCDW is 1.6 Sv during Pandora and nearly zero during MoorSPICE, which is consistent with the model results (within errors) given above. Both nonadjusted and adjusted transports during Pandora confirm that UCDW can enter the Solomon Sea through the southern entrance, although this inflow of UCDW might not be a persistent transport pattern based on the MoorSPICE transport estimates. At the northeastern exit of the Solomon Sea, we find nonadjusted UCDW transports of 1.1 Sv

and -1.8 Sv during Pandora and MoorSPICE, respectively. This is consistent with a pattern of transports in and out of the Solomon Sea Basin above its sill depth (~ 2600 m); nevertheless, the nonadjusted transports during MoorSPICE do not agree with that adjusted through inversion. One possible explanation for this discrepancy may be that, in our model set up with MoorSPICE data, we find quite large vertical velocities (w > 1 x 10^{-4} cm.s^{-1}) across the isopycnals at 27.65 (~ 2000 m) to 27.71 (~ 2500 m) σ_0, indicating the upward transfer of deep water at these densities.

In Alberty et al. (2019), the mean transport through Solomon Strait derived from the SPICE mooring deployment over July 2012 to March 2014 was estimated at 4.6 ± 1.0 Sv **into** the Solomon Sea from 1500 to 2500 m (27.50-27.71 σ_0). During the two SPICE cruises, both the nonadjusted and adjusted transports in the same potential density range (Table S1) indicate an opposite transport pattern (i.e., out of the Solomon Sea Basin) to that determined from the moored observations. The inflow inside the Solomon Sea was mainly found from a mooring deployed in the eastern part of the Solomon Strait (Alberty et al., 2019). The total transport estimate is possibly biased, as the velocities deeper than 1700 m were extrapolated down to 2500 m, and also extrapolated across the Strait (see Alberty et al., 2019 for further detail). Yet, these mooring data provide clear evidence for a persistent throughflow from the East Caroline Basin into the Solomon Sea Basin below 1500 m. This inflow is fully consistent with our conclusions from hydrological properties suggesting the existence of an intrusion of waters through Solomon Strait above σ_0 = 27.73 (see section 4.1). Below, in the potential density layer 27.71-27.76 σ_0, rather small transports (~ 1 Sv; Table S1) are also out of the basin during Pandora, while larger transports (3-5 Sv; Table S1) are into the basin during MoorSPICE. The differences in transports through Solomon Strait are surprising, but they might reflect variations in layer thickness of the deep flow there, associated with significant diapycnal exchanges.

Our model provides layer-to-layer estimates of diffusivity κ_z, however, the obtained diffusion coefficients are not accurate enough (because of too large uncertainties) to draw any conclusion on mixing processes. To gain further insight on mixing in the deep layers of the Solomon Sea, diffusivity can also be inferred using finescale parameterization methods (e.g., Kunze et al., 2006; Polzin et al., 2014). Following the approach of Alberty et al. (2017), we use 320 m long segments of CTD potential density data (from the Pandora and MoorSPICE cruises) to quantify strain variance, which is used to estimate dissipation of kinetic energy (□), which in turn, is used to calculate strain-based estimates of κ_z (Fig. S5). Note that only the CTD casts carried out during the two SPICE cruises at depths greater than 3000 m within the Solomon Sea Basin are considered here. For each segment, the mean squared buoyancy frequency (N^2) is also calculated and estimates of both □ and N^2 from the considered casts (all greater than 3000 m) are bin averaged in 320 m bins over the 2000-4880 m depth range. Average diffusivity $\kappa_{□} = □ \frac{□}{□^2}$, is then estimated using the bin averaged □ and N^2, with an empirical mixing efficiency □ of 0.2 (based on Peltier and Caulfield, 2003). The mean profile of κ_z (Fig. S5) is maximum near 2500 m at 5 x 10^{-4} m^2 s^{-1} and the lowest κ_z values (1-2 x 10^{-6} m^2 s^{-1}) occur at depths below 3750 m. Even

though the error bars of κ_z (grey shading in Fig. S5) are large, these density-derived estimates of κ_z further suggest that diapycnal mixing may play a key role in the transport variability (via layer thickness changes) observed at Solomon Strait between 1500 m to its sill depth near 2600 m.

5 Connection to the Pacific circulation

At 2000 m depth, the historical measurements of θ (Fig. 6a), S (Fig. 6b), O_2 (Fig. 7a) and SiO_4 (Fig. 7b) combined with the corresponding observations from the two SPICE cruises give a consistent picture for the lightest UCDW flow between 20°S to 10°N. There is a region of high-O_2 (> 140 μmol.kg^{-1}), low-SiO_4 (< 130 μmol.kg^{-1}), low-θ and relatively low-S at the southern entrance of the Solomon Sea traced from the Coral Sea Basin. These distinct property distributions can also be traced from the New Caledonia Trough, the New Hebrides Basin and the South Fiji Basin in the southeastern part of the Coral Sea. The South Fiji Basin is connected with the Southwest Pacific Basin via narrow passages at the southern tip of the Tonga-Kermadec Ridge, it is therefore possible that the lightest part of UCDW is also exchanged through these passages between both basins in the potential density range 27.65-27.69 σ_0 (Fig. S6a), before proceeding equatorward. Further north, the water properties of aged UCDW (more O_2-poor and SiO_4-rich than the UCDW south of 10°S) are clearly identified in the East Caroline Basin and the northern part of the Solomon Sea Basin. As discussed in section 4, waters at these depths in the Solomon Sea are a mixture between Coral Sea waters entering from the southern entrance and waters from the East Caroline Basin entering the Solomon Sea through Solomon Strait.

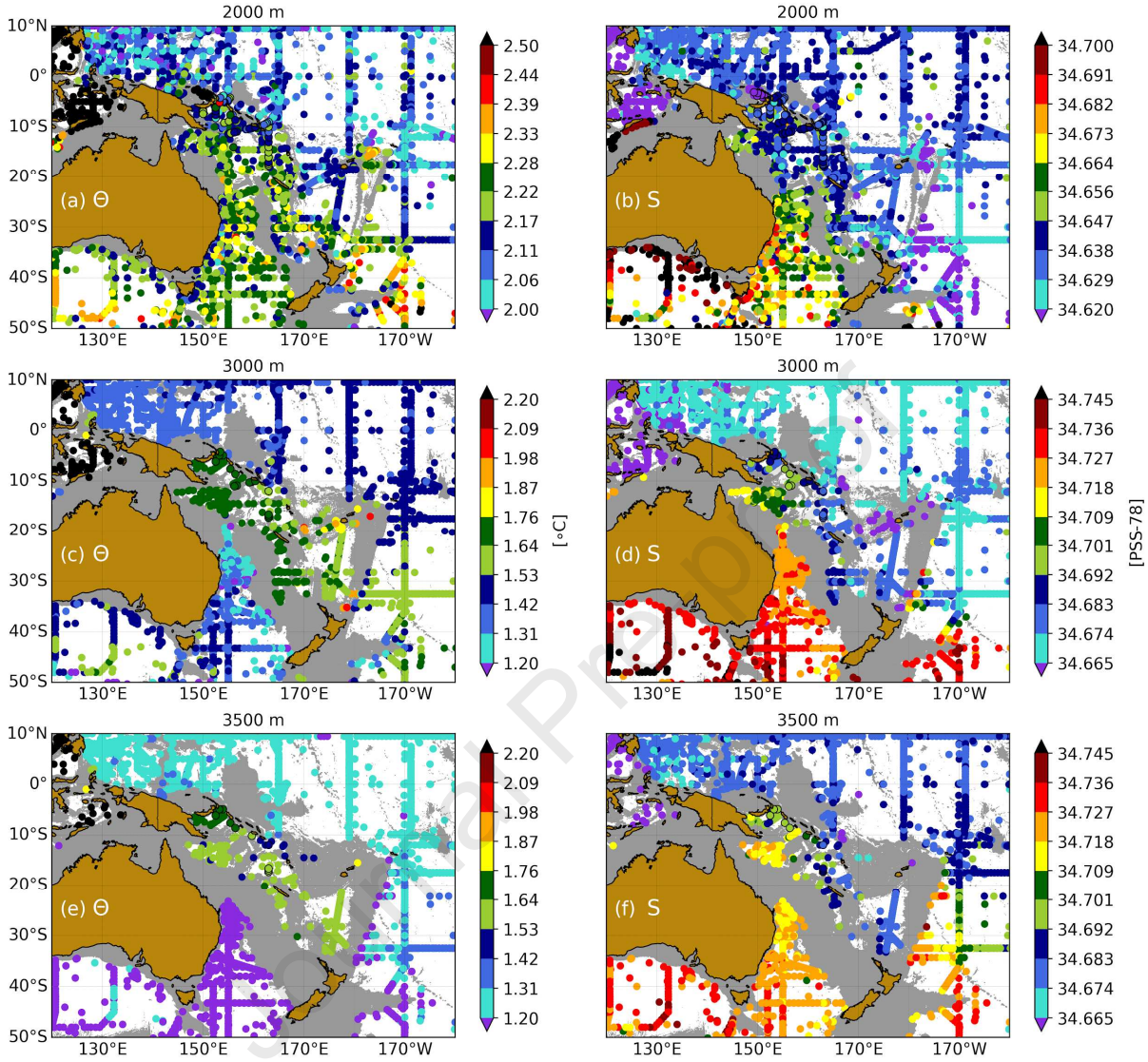

Fig. 6: Historical measurements (colored dots) of (a, c, e) potential temperature θ (°C; referenced to a sea pressure of zero dbar) and (b, d, f) salinity S (PSS-78) from WOA18 at three depth levels encompassing the UCDW, overlaid by the corresponding tracers measured during the two SPICE cruises (colored dots with black outlines). (a, b) show θ and S distributions at 2000 m depth, while (c, d) show similar distributions at 3000 m and (e, f) at 3500 m. In each panel, areas shallower than each corresponding depth level are shaded in gray.

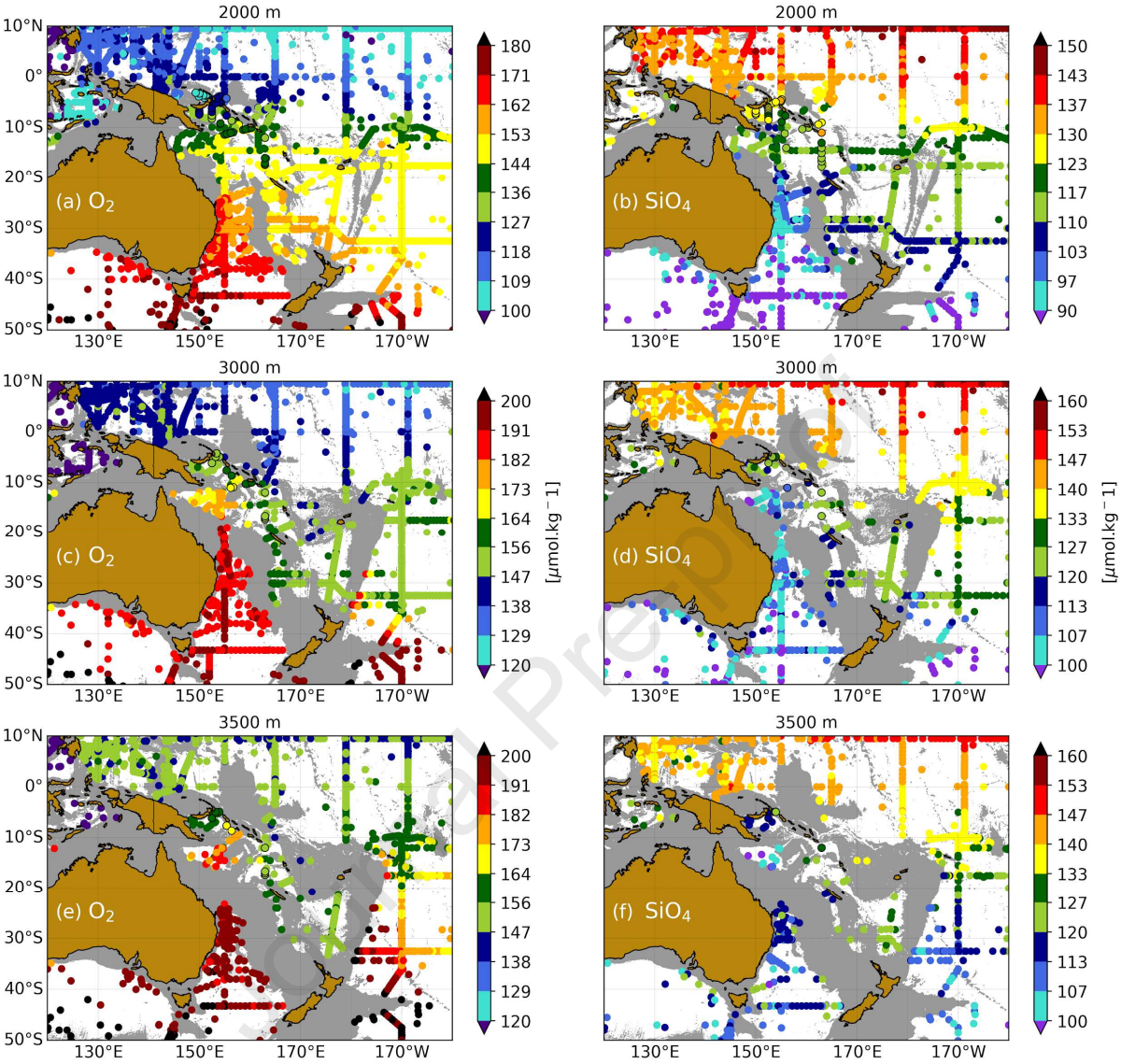

Fig. 7: Historical measurements (colored dots) of (a, c, e) dissolved oxygen O_2 (µmol.kg^{-1}) and (b, d, f) silicate SiO_4 (µmol.kg^{-1}) from WOA18 at three depth levels encompassing the UCDW, as in Fig. 6. The corresponding tracers from the two SPICE cruises are indicated as colored dots with black outlines, and areas shallower than each corresponding depth level are shaded in gray.

At 3000 m depth (Figs. 6c, d and Figs. 7c, d), an inflow of denser UCDW into the Solomon Sea can only happen in the south, East Caroline Basin waters are blocked by topography. As mentioned in section 4.1, UCDW coming from the Coral Sea Basin can enter the Solomon Sea via the Pocklington Trough, while UCDW emanating from the New Hebrides and the South Fiji Basins can enter the Solomon Sea Basin. UCDW inflow originating from the New Caledonia Trough might also occur. The property distributions support this view, although UCDW in the Coral Sea Basin is, for similar θ classes (Fig. 6c), saltier (Fig. 6d), more O_2-rich (Fig. 7c) and SiO_4-poor (Fig. 7d) than UCDW originating from the New Hebrides and the South Fiji Basins.

This pattern of high-O_2 and low-SiO_4 possibly reflects changes in the UCDW layer thickness (and thus diapycnal exchange), allowing an upwelling of UCDW from the East Australian Basin, which is closed to the north below 2850 m, into the Coral Sea Basin. Both UCDW from these sources flow towards each other with similar potential densities (Fig. S6b), and possibly mix around the southern entrance of the Solomon Sea before proceeding northward into the Solomon Sea. The New Caledonia Trough is closed to the north below 3000 m, while the Tonga-Kermadec Ridge prevents possible throughflow coming from the Southwest Pacific Basin (Fig. 2).

At 3500 m depth, the distributions of θ (Fig. 6e), S (Fig. 6f) O_2 (Fig. 7e) and SiO_4 (Fig. 7f) indicate that the Solomon Sea Basin is filled by lighter UCDW coming from the Coral Sea Basin. So, even if the Solomon Sea Basin is still connected to the Coral Sea Basin via the Pocklington Trough and to the New Hebrides Basin and the South Fiji Basin via the South Solomon Trench, these passages are too narrow to allow significant transport of UCDW into the Solomon Sea, which is consistent with our findings outlined in section 4.1. Most importantly, it is clear that the apparent high-O_2 signature found at the deepest stations in the Solomon Sea Basin do originate from the high-O_2 Coral Sea waters, and extend deeper below waters with lower O_2. At 4000 m depth, the Coral Sea Basin is no longer connected to the east by the Pocklington Trough and we find, overall, similar water property distributions (Figs. 8a, b and 9a, b) than those at 3500 m from the South Fiji Basin to the Solomon Sea Basin.

At 4500 m depth, the southern part of the South Fiji Basin appears to be disconnected with the northwestern part of the South Pacific, and only minor changes in property values are observed (Figs. 8c, d and 9c, d). Below 4500 m, the South Fiji Basin is closed, and the circulation is strongly constrained by the sharp and complex topography over the three main trenches of the Southwest Pacific: the New Hebrides Trench east of New Caledonia, the South Solomon Trench that runs along the Solomon Islands and the New Britain Trench in the Solomon Sea. However, the question arises as to whether there is possible throughflow along this complex trench system, as only scattered measurements are available from WOA18 (Figs. 8e, f and 9e, f).

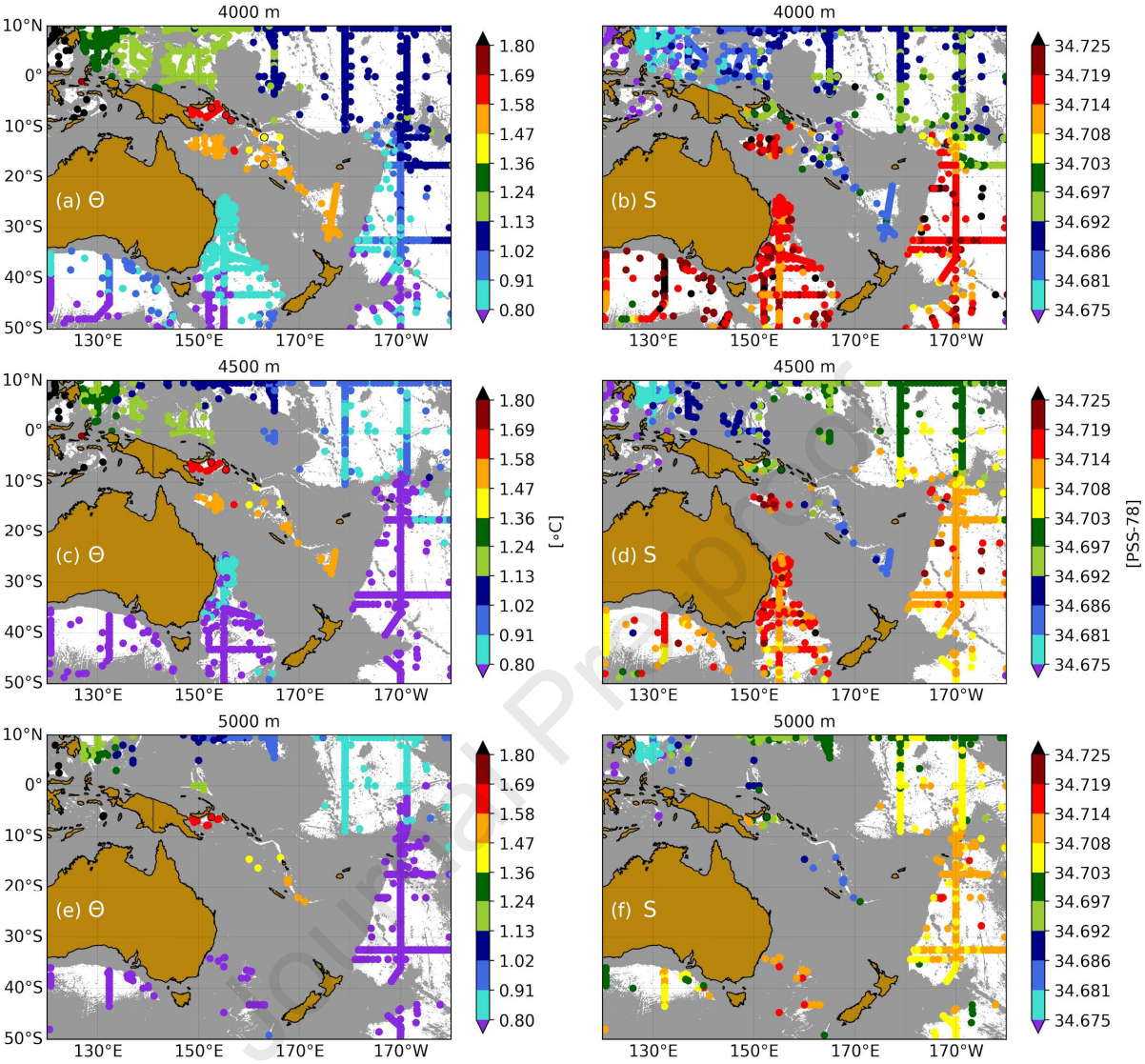

Fig. 8: Historical measurements (colored dots) of (a, c, e) potential temperature θ (°C; referenced to a sea pressure of zero dbar) and (b, d, f) salinity S (PSS-78) from WOA18 at three depth levels encompassing the LCDW. (a, b) show θ and S distributions at 4000 m depth, while (c, d) show similar distributions at 4500 m and (e, f) at 5000 m. The corresponding tracers from the two SPICE cruises are indicated as colored dots with black outlines, and areas shallower than each corresponding depth level are shaded in gray.

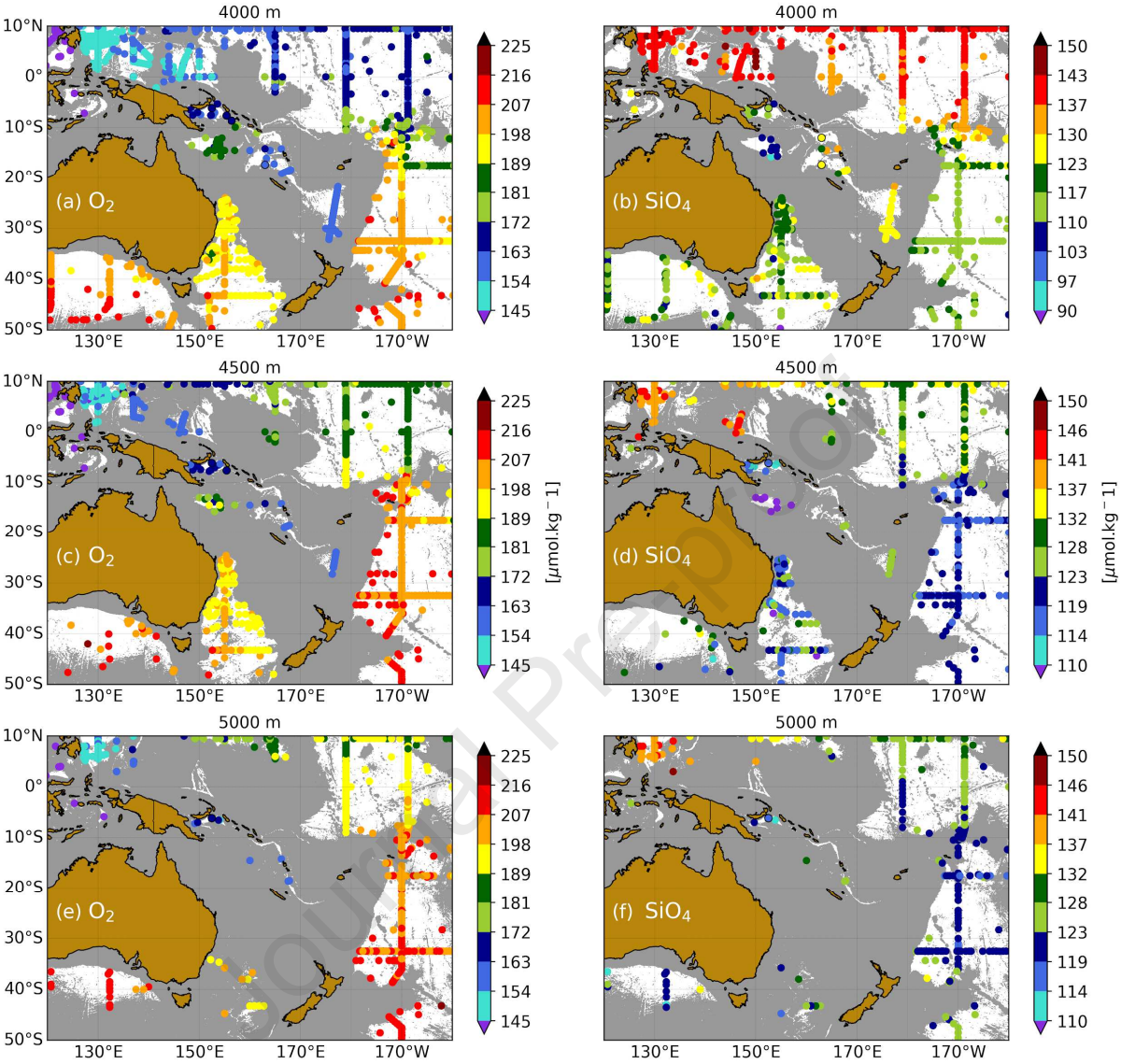

Fig. 9: Historical measurements (colored dots) of (a, c, e) dissolved oxygen O_2 (µmol.kg^{-1}) and (b, d, f) silicate SiO_4 (µmol.kg^{-1}) from WOA18 at three depth levels encompassing the LCDW, as in Fig. 8. The corresponding tracers from the two SPICE cruises are indicated as colored dots with black outlines, and areas shallower than each corresponding depth level are shaded in gray.

The preservation of the water properties below 3500 m in these basins and trenches further indicates that only the densest part of UCDW, which is more O_2-rich than the upper part, supplies the bottom water in both the Coral and Solomon Seas. The potential density distributions at 3500 to 4500 m depths (Figs. S6c-f) show little regional variation, with denser water in the Coral Sea Basin compared to that in the Solomon Sea Basin, the New Hebrides and the South Fiji Basins. This indicates that locally in each basin, horizontal mixing processes play only a minor role in determining the deep water mass structure, and also that the differences in

SiO_4 and O_2 within the Solomon Sea likely reflect the aging gradient of dense UCDW coming from the Coral Sea Basin, as suggested in section 4.1.

6 Concluding remarks

Our understanding of the global deep and abyssal circulation is, for the most part, still limited to scattered observations in both space and time from hydrographic sections. In the Subtropical Pacific, the deep water mass distributions are well-known to be mostly influenced by the UCDW at depths between 2000 to 3500 m, while below, a pattern of higher S, lower SiO_4 and increasing values of O_2 indicates the influence of the LCDW. However, the presence and fate of both water masses in the Coral and Solomon Seas, located in the Southwest Pacific west of the Tonga-Kermadec Ridge remained poorly documented. This is largely due to the intricate bathymetric features and remote deep ocean basins found in the region, which make it challenging to discern the pathways of deep flow and exchanges in the region.

Using direct measurements of water properties from three cruises combined with WOA18 historical data, this study examined the origin, the characteristics and pathways of the deep flow pattern in the Solomon Sea, and discusses their origin. Our results indicate that UCDW entering the Solomon Sea Basin through the southern entrance primarily comes from the Coral Sea Basin rather than the Central Pacific Basin, as proposed by Wyrtki (1961). At depths between 2000 and 3000 m, the UCDW signature reaches as far as the New Caledonia Trough and the southernmost part of the South Fiji Basin, located west of the Tonga-Kermadec Ridge. The water property distributions indicate water mass modifications in the northern part of the Solomon Sea Basin between the southern UCDW and a flow of older and/or modified UCDW emanating from the East Caroline Basin at depths shallower than 2600 m (~ 27.73 σ_0), bringing fresher, O_2-poor and SiO_4-rich waters into the Solomon Sea Basin through Solomon Strait. The Solomon Sea is thus, at these depths, a region where both types of UCDW (with respectively southern and northern origins) can mix.

During the MoorSPICE cruise, water properties were collected at great depths in the Bismarck Sea (~ 147.3°E-150.8°E, 2.7°S-5.2°S), and clearly indicate that, below 1750 m, the Bismarck Sea is completely isolated from the large scale deep western boundary circulation in the western equatorial Pacific. Despite this lack of ventilation, the constant values of the oxygen and nutrients suggest either an absence of remineralization at depth in this closed basin, or little remineralization that is gradually compensated by downward diffusion of oxygen. In the 3000-3500 m depth range, the Solomon Sea Basin is still filled by UCDW inflow directly coming from the Coral Sea Basin via a deep channel (the Pocklington Trough), and probably the UCDW that meanders from the New Hebrides and the South Fiji Basins. The deep water mass properties suggest that both UCDW inflows approach each other at the southern entrance of the Solomon Sea Basin, from where a mixture between the two UCDW appears to proceed equatorward into the northern part of the basin. There, the concentrations of O_2 increase with depth between 3000

to 3500 m, indicating that the densest part of UCDW imprints the high-O_2 feature of LCDW. Below 3500 m, the water column is locally vertically homogeneous in the Solomon Sea Basin, suggesting that only UCDW supplies the near-bottom levels in the basin. This is consistent with the GEBCO 2020 bathymetric data, which indicates that LCDW is prevented by topography from spreading to the Southwest Pacific basins. In addition, the lack of oxygen consumption below 3500 m in the Solomon Sea Basin suggests that there is little or no remineralization at depth.

The adjusted transports estimated by inversion across the Solomon Sea are overall consistent with this circulation scheme inferred from the water properties, despite some differences in transport estimates between the Pandora and MoorSPICE cruises. We found an equatorward transport of 5 ± 2.6 Sv during Pandora (in July 2012) over 27.50-27.76 σ_0 (~ 1500-3250 m), whereas weaker (1 ± 1.9 to 2.4 ± 1.6 Sv) transports were found during MoorSPICE (March 2014) at those densities. At Solomon Strait, the estimated transport over 27.71-27.76 σ_0 (~ 2500-3250 m) is close to zero (within errors) during Pandora, while a southward transport of 3 ± 0.8 Sv is found during MoorSPICE. Although the Solomon Sea Basin is closed to the north below a sill depth of about 2600 m, these transport estimates provide evidence for some throughflow variability between the East Caroline and Solomon Sea Basins from 1500 m depth to the 2600 m sill-depth, which is consistent with the water mass property changes observed there. Estimates of diapycnal velocity and mixing further indicate that significant diapycnal exchanges occur throughout the Solomon Sea Basin below 2000 m depth, influencing both the water mass structure and transports of the deep flow across the basin.

Deeper in the water column, the abyssal flow (> 4000 m) west of the Tonga-Kermadec Ridge is strongly constrained by a complex system of long and narrow deep trenches beginning southeast of New Caledonia, which then border the southern coastline of the Solomon Islands extending to the South Solomon Trench. The overall distribution of the corresponding water mass properties (i.e., θ, S, O_2 and SiO_4) is based only on a few historical profiles; it is, therefore, difficult to rely only on these water properties to explore the abyssal water mass structure and associated flow paths over these trenches. One may use geochemical tracers such as trace elements and isotopes to further characterize the near-bottom waters in these remote deep trenches. Nevertheless, more water property observations are required to thoroughly detail the deep and abyssal water mass distributions in the region. To this end, the recent extension of the Argo array below the typical 2000 m sampling limit in the Southwest Pacific Basin (Johnson et al., 2019) offers hope for additional insights into the deep and abyssal circulation in the region.

Acknowledgments
The two exploratory cruises known as Pandora and MoorSPICE are contributions to the CLIVAR/SPICE and GEOTRACES International programs. The Pandora cruise has been co-funded by ANR (project ANR-09- BLAN-0233-01) and INSU/LEFE project Solwara, while the MoorSPICE cruises has been funded by the NSF grant OCE1029487. The data collected during Pandora and MoorSPICE are available online at http://www.obs-vlfr.fr/proof/cruises.php. MoorSPICE data can also be found online at https://doi.org/10.7284/903044. We thank the crews of the R/V Atalante and R/V Thomas G. Thompson. We are grateful to the engineers from the Institut de Recherche pour le Développement (IRD) US-IMAGO team, DT-INSU and Scripps Institution of Oceanography (SIO), and scientists who carefully sampled, recorded, and treated the data. Ocean historical data were freely downloaded from the World Ocean Atlas 2018 (WOA18) database (https://www.nodc.noaa.gov/OC5/woa18). We also thank Catherine Jeandel, Valérie Chavagnac, Louis Géli and Cédric Boulart for fruitful discussions concerning the deepest water mass properties. The gridded 30 arc-second General Bathymetric Chart of the Oceans (GEBCO) 2020 bathymetry was also freely downloaded from GEBCO's website (https://www.gebco.net). Cyril Germineaud's work on this study was carried out in part under the auspices of the Cooperative Institute for Marine and Atmospheric Studies (CIMAS), a Cooperative Institute of the University of Miami and the National Oceanic and Atmospheric Administration (NOAA), cooperative agreement NA20OAR4320472. Cyril Germineaud also acknowledges support from the NOAA Atlantic Oceanographic and Meteorological Laboratory.

References

Alberty, M. S., J. Sprintall, J. MacKinnon, A. Ganachaud, S. Cravatte, G. Eldin, C. Germineaud, and A. Melet (2017), Spatial patterns of mixing in the Solomon Sea, *Journal of Geophysical Research: Oceans,* 122(5), 4021-4039.

Alberty, M., Sprintall, J., MacKinnon, J., Germineaud, C., Cravatte, S., & Ganachaud, A. (2019). Moored Observations of Transport in the Solomon Sea. *Journal of Geophysical Research: Oceans*, 124(11), 8166-8192.

Alford, M. H., J. B. Girton, G. Voet, G. S. Carter, J. B. Mickett, and J. M. Klymak (2013), Turbulent mixing and hydraulic control of abyssal water in the Samoan Passage, *Geophysical Research Letters,* 40(17), 4668-4674.

Callahan, J. E. (1972), The structure and circulation of deep water in the Antarctic, *Deep Sea Research and Oceanographic Abstracts*, 19(8), 563-575.

Cazenave, A., & Llovel, W. (2010). Contemporary sea level rise. *Annual review of marine science*, *2*, 145-173.

Delpech, A., Cravatte, S., Marin, F., Morel, Y., Gronchi, E., & Kestenare, E. (2020). Observed Tracer Fields Structuration by Middepth Zonal Jets in the Tropical Pacific. *Journal of Physical Oceanography*, 50(2), 281-304.

Desbruyères, D. G., Purkey, S. G., McDonagh, E. L., Johnson, G. C., & King, B. A. (2016). Deep and abyssal ocean warming from 35 years of repeat hydrography. *Geophysical Research Letters*, 43(19), 10-356.

Ganachaud, A., & Wunsch, C. (2000). Improved estimates of global ocean circulation, heat transport and mixing from hydrographic data. *Nature*, 408(6811), 453-457.

Ganachaud, A. (2003), Error budget of inverse box models: The North Atlantic, *Journal of Atmospheric and Oceanic Technology, 20*(11), 1641-1655.

Ganachaud, A., Cravatte, S., Sprintall, J., Germineaud, C., Alberty, M., Jeandel, C., ... & Heimburger, L. E. (2017). The Solomon Sea: its circulation, chemistry, geochemistry and biology explored during two oceanographic cruises, *Elem. Sci. Anth.*, 5, 33.

Germineaud, C., A. Ganachaud, J. Sprintall, S. Cravatte, G. Eldin, M. S. Alberty, and E. Privat (2016), Pathways and water mass properties of the thermocline and intermediate waters in the Solomon Sea, *Journal of Physical Oceanography, 46*(10), 3031-3049.

Halunen Jr, A. J., & Von Herzen, R. P. (1973). Heat flow in the western equatorial Pacific Ocean. *Journal of Geophysical Research*, *78*(23), 5195-5208.

Hood, E., C. Sabine, and B. Sloyan (2010), The go-ship repeat hydrography manual: A collection of expert reports and guidelines, IOCCP Rep, 14.

Johnson, G. C. (2008), Quantifying Antarctic Bottom Water and North Atlantic deep water volumes, *Journal of Geophysical Research: Oceans, 113*(C5), c05027.

Johnson, G. C., and J. M. Toole (1993), Flow of deep and bottom waters in the Pacific at 10°N, *Deep Sea Research Part I: Oceanographic Research Papers*, 40, 371-394.

Johnson, H. P., Hautala, S. L., Bjorklund, T. A., & Zarnetske, M. R. (2006). Quantifying the North Pacific silica plume. *Geochemistry, Geophysics, Geosystems*, 7(5).

Johnson, G. C., J. M. Lyman, and S. G. Purkey (2015), Informing deep argo array design using argo and full-depth hydrographic section data, *Journal of Atmospheric and Oceanic Technology*, 32(11), 2187-2198.

Johnson, G. C., Purkey, S. G., Zilberman, N. V., & Roemmich, D. (2019). Deep Argo quantifies bottom water warming rates in the Southwest Pacific Basin. *Geophysical Research Letters*, 46(5), 2662-2669.

Joshima, M., & Honza, E. (1986). Age estimation of the Solomon Sea based on heat flow data. *Geo-marine letters*, *6*(4), 211-217.

Kawabe, M., and S. Fujio (2010), Pacific Ocean circulation based on observation, *Journal of Oceanography*, 66(3), 389-403.

Kawabe, M., D. Yanagimoto, and S. Kitagawa (2006), Variations of deep western boundary currents in the melanesian basin in the western North Pacific, *Deep Sea Research Part I: Oceanographic Research Papers*, 53(6), 942-959.

Kawabe, M., S. Fujio, D. Yanagimoto, and K. Tanaka (2009), Water masses and currents of deep circulation southwest of the Shatsky Rise in the western North Pacific, *Deep Sea Research Part I: Oceanographic Research Papers*, 56(10), 1675-1687.

Kunze, E., Firing, E., Hummon, J. M., Chereskin, T. K., & Thurnherr, A. M. (2006). Global abyssal mixing inferred from lowered ADCP shear and CTD strain profiles. *Journal of Physical Oceanography*, 36(8), 1553-1576.

Langdon, C. (2010), Determination of dissolved oxygen in Seawater by Winkler Titration using the Amperometric Technique, The GO-SHIP Repeat Hydrography Manual: A Collection of Expert Reports and Guidelines IOCCP Report no 14, GO-SHIP.ORG, version1.

Lindstrom, E., R. Lukas, R. A. Fine, J. S. Godfrey, G. Meyers, and M. Tsuchiya, 1987: The Western Equatorial Pacific Ocean Circulation Study. *Nature*, 330, 533–537.

Lumpkin, R., & Speer, K. (2007). Global ocean meridional overturning. *Journal of Physical Oceanography*, 37(10), 2550-2562.

Mantyla, A. W., and J. L. Reid (1983), Abyssal characteristics of the world ocean waters, *Deep Sea Research Part A. Oceanographic Research Papers*, 30(8), 805-833.

Meinen, C. S., Perez, R. C., Dong, S., Piola, A. R., & Campos, E. (2020). Observed ocean bottom temperature variability at four sites in the northwestern Argentine Basin: Evidence of decadal deep/abyssal warming amidst hourly to interannual variability during 2009-2019. *Geophysical Research Letters*, e2020GL089093.

Melet, A., J. Verron, L. Gourdeau, and A. Koch-Larrouy (2011), Equatorward pathways of Solomon Sea water masses and their modifications, *Journal of Physical Oceanography,* 41, 810-826.

Orsi, A. H., G. C. Johnson, and J. L. Bullister (1999), Circulation, mixing, and production of Antarctic Bottom Water, *Progress in Oceanography,* 43(1), 55-109.

Peltier, W. R., & Caulfield, C. P. (2003). Mixing efficiency in stratified shear flows. *Annual review of fluid mechanics*, 35(1), 135-167.

Polzin, K. L., Garabato, A. C. N., Huussen, T. N., Sloyan, B. M., & Waterman, S. (2014). Finescale parameterizations of turbulent dissipation. *Journal of Geophysical Research: Oceans*, 119(2), 1383-1419.

Purkey, S. G., & Johnson, G. C. (2010). Warming of global abyssal and deep Southern Ocean waters between the 1990s and 2000s: Contributions to global heat and sea level rise budgets. *Journal of Climate*, 23(23), 6336-6351.

Purkey, S. G., Johnson, G. C., Talley, L. D., Sloyan, B. M., Wijffels, S. E., Smethie, W., et al. (2019). Unabated Bottom Water Warming and Freshening in the South Pacific Ocean. *Journal of Geophysical Research: Oceans*, 124, 1778-1794.

Reid, J. L. (1986), On the total geostrophic circulation of the south Pacific Ocean: Flow patterns, tracers and transports, *Progress in Oceanography,* 16(1), 1-61.

Reid, J. L. (1997), On the total geostrophic circulation of the Pacific Ocean: flow patterns, tracers, and transports, *Progress in Oceanography,* 39(4), 263-352.

Ridgway, K., J. Dunn, and J. Wilkin (2002), Ocean interpolation by four-dimensional weighted least squares-application to the waters around Australia, J*ournal of atmospheric and oceanic technology, 19*(9), 1357-1375.

Roemmich, D., S. Hautala, and D. Rudnick (1996), Northward abyssal transport through the Samoan Passage and adjacent regions, *Journal of Geophysical Research: Oceans, 101(*C6), 14,039-14,055.

Rudnick, D. L. (1997), Direct velocity measurements in the Samoan Passage, *Journal of Geophysical Research: Oceans, 102*(C2), 3293-3302.

Saout-Grit, C., A. Ganachaud, C. Maes, L. Finot, L. Jamet, F. Baurand, and J. Grelet (2015), Calibration of CTD oxygen data collected in the Coral Sea during the 2012 bifurcation cruise, Mercator Ocean-Coriolis Quarterly Newsletter Special Issue, 52(3), 27-33.

Siedler, G., J. Holfort, W. Zenk, T. J. Müller, and T. Csernok (2004), Deep-Water flow in the Mariana and Caroline Basins, *Journal of Physical Oceanography*, *34*(3), 566-581.

Sokolov, S., and S. Rintoul (2000), Circulation and water masses of the southwest Pacific: WOCE section P11, Papua New Guinea to Tasmania, *Journal of marine research*, 58(2), 223-268.

Taft, B. A., S. P. Hayes, G. E. Friederich, and L. A. Codispoti (1991), Flow of abyssal water into the Samoa Passage, *Deep Sea Research Part A. Oceanographic Research Papers*, 38, S103-S128.

Talley, L. D., and T. M. Joyce (1992), The double silica maximum in the North Pacific, *Journal of Geophysical Research: Oceans*, 97(C4), 5465-5480.

Talley, L. D., M. D. Sparrow, P. Chapman, and J. Gould (2007), Hydrographic atlas of the World Ocean Circulation Experiment (WOCE): Volume 2: Pacific Ocean, WOCE International Project Office.

Toole, J. M., R. W. Schmitt, and K. L. Polzin (1994), Estimates of diapycnal mixing in the abyssal ocean, *Science*, 264(5162), 1120.

Tsimplis, M. N., S. Bacon, and H. L. Bryden (1998), The circulation of the subtropical South Pacific derived from hydrographic data, *Journal of Geophysical Research: Oceans*, 103(C10), 21,443-21,468.

Tsuchiya, M. (1991). Flow path of the Antarctic Intermediate Water in the western equatorial South Pacific Ocean. *Deep Sea Research Part A. Oceanographic Research Papers*, 38, S273-S279.

Uchida, H., C. G. Johnson, and K. E. McTaggart (2010), CTD oxygen sensor calibration procedures, The GO-SHIP Repeat Hydrography Manual: A Collection of Expert Reports and Guidelines IOCCP Report no 14, GO-SHIP.ORG, version 1.

Visbeck, M. (2002), Deep velocity profiling using Acoustic Doppler Current Profilers: Bottom tracks and inverse solutions., *Journal of Atmospheric and Oceanic Technology*, 19, 794-807.

Voet, G., J. B. Girton, M. H. Alford, G. S. Carter, J. M. Klymak, and J. B. Mickett (2014), Pathways, volume transport, and mixing of abyssal water in the Samoan Passage, *Journal of Physical Oceanography*, 45(2), 562-588.

Voet, G., M. H. Alford, J. B. Girton, G. S. Carter, J. B. Mickett, and J. M. Klymak (2016), Warming and weakening of the abyssal flow through Samoan Passage, *Journal of Physical Oceanography*, 46(8), 2389-2401.

Warren, B. A. (1973), Transpacific hydrographic sections at Lats. 43°S and 28°S: the SCORPIO expedition II. deep water, *Deep Sea Research and Oceanographic Abstracts*, 20(1), 9-38.

Whitworth III, T., B. A. Warren, W. D. Nowlin, Jr, S. B. Rutz, R. D. Pillsbury, and M. I. Moore (1999), On the deep western-boundary current in the southwest Pacific Basin, *Progress in Oceanography*, 43(1), 1-54.

Wijffels, S. E., M. M. Hall, T. Joyce, D. J. Torres, P. Hacker, and E. Firing (1998), Multiple deep gyres of the western North Pacific: A woce section along 149°E, *Journal of Geophysical Research: Oceans*, 103(C6), 12, 985-13,009.

Wijffels, S. E., J. M. Toole, and R. Davis (2001), Revisiting the south pacific subtropical circulation: A synthesis of world ocean circulation experiment observations along 32°S, *Journal of Geophysical Research: Oceans*, 106(C9), 19, 481-19,513.

Wunsch, C. (1996). *The ocean circulation inverse problem*. Cambridge University Press, 442 pp.

Wyrtki, K. (1961). The flow of water into the deep sea basins of the western South Pacific Ocean. *Marine and Freshwater Research*, 12(1), 1-16.

Declaration of interests

● The authors declare that they have no known competing financial interests or personal relationships that could have appeared to influence the work reported in this paper.

☐The authors declare the following financial interests/personal relationships which may be considered as potential competing interests: